Selectins impair regulatory T cell function and contribute to systemic lupus erythematosus pathogenesis

Marc Scherlinger, Vivien Guillotin, Isabelle Douchet, Pierre Vacher, Andréa Boizard-Moracchini, Jean-Philippe Guegan, Anne Garreau, Nathalie Merillon, Agathe Vermorel, Emmanuel Ribeiro, et al.

Selectins impair regulatory T cell function and contribute to systemic lupus erythematosus pathogenesis

Short title : Selectins impair Tregs in systemic lupus

Authors : Marc Scherlinger[1,2,3] , Vivien Guillotin[2,3,4], Isabelle Douchet[3] , Pierre Vacher[5], Andrea Boizard[3], Jean Philippe Guegan[6], Anne Garreau[3], Nathalie Merillon[3], Agathe Vermorel[7], Emmanuel Ribeiro[4], Irène Machelart[2,8], Estibaliz Lazaro[2,8], Lionel Couzi[7], Pierre Duffau[8], Thomas Barnetche[1,2], Jean-Luc Pellegrin[2,8], Jean-François Viallard[2,8], Maya Saleh[3], Thierry Schaeverbeke[1,2,], Patrick Legembre[9], Marie-Elise Truchetet[1,2,3], Hélène Dumortier[10], Cécile Contin-Bordes[3,10], Vanja Sisirak[3], Christophe Richez* [1,2,3] & Patrick Blanco* [2,3,11]

Affiliations:
[1] Department of Rheumatology, Pellegrin, Bordeaux University Hospital, France.
[2] Centre national de référence maladie auto-immune et systémique rares Est/Sud-Ouest (RESO).
[3] UMR-CNRS 5164, ImmunoConcept, University of Bordeaux, France.
[4] Department of Internal Medicine, Saint André, Bordeaux University Hospital, France.
[5] INSERM U1218, Bordeaux, France.
[6] CLCC Eugène Marquis, Inserm U1242, Equipe Ligue Contre Le Cancer, 35042 Rennes, France.
[7] Nephrology department, Bordeaux University Hospital, France.
[8] Department of Internal Medicine, Haut-Leveque, Bordeaux University Hospital, France.
[9] Explicyte SAS,229 Cours de l'Argonne, 33000 Bordeaux
[10]
[11] Department of Immunology and Immunogenetics, Bordeaux University Hospital, France.

Corresponding authors:
Prof Patrick Blanco, MD. PhD. ** Lead contact
Department of Immunology and Immunogenetics, Pellegrin, Bordeaux University Hospital, place Amélie Raba Léon, 33076 Bordeaux, France.
Email: patrick.blanco@chu-bordeaux.fr
Phone: +33 556795679
Fax: +33 557820937

Prof Christophe Richez, MD. PhD
Department of Rheumatology, Pellegrin, Bordeaux University Hospital, place Amélie Raba Léon, 33076 Bordeaux, France.
Email: christophe.richez@chu-bordeaux.fr
Phone: +33 556795483
Fax: +33 557820937

*, Participated equally.

Summary:

Systemic lupus erythematosus (SLE) is a systemic autoimmune disease characterized by a loss of tolerance toward self-nucleic acids, autoantibody production, an interferon signature, and a defect in the T regulatory cells (Tregs) compartment. In this work, we identified that platelets from active SLE patients preferentially interacted with Tregs *via* the P-selectin/PSGL-1 axis. Selectin interaction with PSGL-1 blocked the regulatory/suppressive properties of Tregs and follicular Tregs by triggering Syk phosphorylation and an increase in intracytosolic calcium. Mechanistically, P-selectin engagement on Tregs induced a downregulation of the TGF-beta axis, altering Tregs phenotype and limiting their immunosuppressive response. In patients, we found a significant upregulation of P- and E-selectin levels both expressed by microparticles and in their soluble forms that correlated with SLE disease activity. Finally, blocking P-selectin in a mouse model of SLE improved cardinal features of the disease. Overall, our results identify a selectin-dependent pathway active in SLE patients and validate it as a potential therapeutic avenue.

Keywords: systemic lupus erythematosus; selectin; PSGL-1; T regulatory lymphocytes; platelets; autoimmune disease

Introduction:

Systemic lupus erythematosus (SLE) is an autoimmune disease characterized by a loss of tolerance against self-nucleic acids and type I interferon production *(1)*. Self-reactive B cells primed by interferons are responsible for auto-antibody production, immune complex formation and deposition in tissues, leading to end-organ disease. Previously most targeted therapies were directed against B cells or interferons *(2)*. However, the vast majority of these drugs did not reach significant efficacy endpoints in human clinical trials, indicating that alternative therapeutic strategies should be considered. Along these lines, the role of effector T cells including follicular helper T cells, known for their ability to induce germinal center responses, and regulatory T cells (Tregs), which dampen immune responses, have been highlighted and could represent therapeutic opportunities *(3)*.

Foxp3$^+$ Tregs are important for the maintenance of immunological tolerance, and their absence or deregulation results in fatal autoimmune diseases in humans and mice *(3)*. In SLE, defects in the Treg compartment have been observed both in mouse models and patients *(3)*. Importantly, failure of Tregs to control exaggerated T and B cell activation in SLE may depend on cell-extrinsic factors, including the interplay of Tregs with other immune cells in the inflammatory milieu. As an example, we, and others, have recently identified the ability of OX40L-expressing monocytes, activated by immune complexes (ICs), to induce the differentiation of naïve and memory T cells into B-helper cells *(4, 5)*, while inhibiting the immunosuppressive properties of Tfr and Tregs *(6)*. ICs also influence the function of several cells of the innate immune system, including neutrophils and platelets. Blood platelets, typically involved in primary hemostasis, are activated in several autoimmune disorders and constitute an adjuvant factor in autoimmunity through their ability to tightly interact with other cells by the formation of platelet/cell aggregates *(7, 8)*. In SLE patients, platelets express high levels of P-selectin, are activated by circulating ICs, form aggregates with pDCs and promote the secretion of type I interferon by pDCs in a CD40/CD40L-dependent mechanism ultimately contributing to SLE pathogenesis *(9)*.

Selectins play an important role in the migration of circulating leukocytes to the site of inflammation. During inflammation, P- and E-selectins are upregulated on platelets and endothelial cells and mediate cell adhesion under flow, therefore playing a crucial role in the immune response *(10)*. Accordingly, selectins are elevated at both the tissue and circulating levels in many inflammatory conditions, including sepsis and atherosclerosis *(11–13)*. Selectins bind to P-selectin glycoprotein ligand-1 (PSGL-1), which is an adhesion molecule expressed by many types of hematopoietic cells including T cells. The binding of selectins to PSGL-1 depends on its post-translational modifications such as fucosylation that inserts a sialyl-lewis X motif (sLe^x). sLe^x, designated as cluster of differentiation 15s (CD15s), is a tetrasaccharide carbohydrate usually fused to O-glycans *(14)*. Although PSGL-1 has long been studied as an adhesion molecule involved in immune cell trafficking, it is now increasingly recognized as a regulator of many aspects of the immune response *(15, 16)*. Strikingly, we confirmed that among lymphoid cells, Tregs and Tfr express the highest levels of PSGL-1/CD15s, potentially conferring a specific platelet/selectin interaction *(17)*. Since SLE is characterized by platelet activation that induces P-selectin exposure and secretion, we asked whether Treg function is affected by platelets in SLE patients.

Here, we found that P-selectin impairs the immunosuppressive functions of Tregs and Tfr cells. Mechanistically, through binding to CD15s-associated PSGL-1, selectins induced a Syk-dependent calcium increase, decreased GARP expression, TGF-beta release and Foxp3 expression. We show that soluble P-selectin, P-selectin-associated microparticles, and platelet-Treg aggregates have the strongest association with disease severity in SLE patients. In a mouse model of SLE, P-selectin blockade attenuated disease severity. Collectively, our results provide clinical and functional evidence of the role of P-selectin in SLE pathogenesis and point to P-selectin as a valuable therapeutic target in SLE patients.

Results:

Tregs and Tfr express high level of fucosylated (CD15s) PSGL-1

In SLE patients, platelets have an activated phenotype in relation to disease activity and severity *(8)*, and the relocation of P-selectin on the platelet membrane is a hallmark of platelet activation *(10)*. To investigate which immune cell populations interacted with P-selectin-expressing platelets, we first analyzed PSGL-1 expression using flow cytometry on fresh blood samples. In healthy donors (HD), PSGL-1 expression was highest on plasmacytoid dendritic cells (pDCs), moderate on myeloid dendritic cells (mDCs), monocytes, granulocytes and T cells, and nearly absent on B lymphocytes (**figure 1A**; gating strategy see **figure S1A**). Among T lymphocyte subpopulations, $CD4^+$ $CD25^{high}$ $CD127^{low}$ T regulatory cells (Tregs) showed the highest expression of PSGL-1 compared to other subpopulations ($p < 0.0001$, **figure 1B**; gating strategy see **figure S1B**). Since PSGL-1 fucosylation is necessary for its interaction with its receptor (e.g., selectins), we next monitored CD15s expression at the plasma membrane of circulating leukocytes in HD. We observed that among T cells, Tregs (specifically $CD45RA^-$ $FoxP3^+$) expressed higher levels of CD15s compared to Teff cells ($p < 0.001$, **figures S1D and S1E**). Interestingly, the Tfr population $CD3^+$ $CD45RA^-$ $CXCR5^+$ $Foxp3^+$ $CD25^+$ also expressed high levels of CD15s (**figures S1D and S1E**). In SLE patients, both resting ($CD45RA^+$) and effector ($CD45RA^-$) $FoxP3^{high}$ Tregs expressed significantly higher PSGL-1 (**figure 1C,** gating shown in **figure S1C**) and CD15s (**figure S1F**) levels than T effector lymphocytes. Tregs from SLE and HD expressed similar levels of PSGL-1 and CD15s (**figure S1G**).

We next explored whether CD15s-expressing Tregs interacted with platelets in HD and SLE patients. Using flow cytometry, circulatory platelet/Treg aggregates (defined as $CD61^+$[platelet]/$CD4^+CD127^-CD25^+$[Treg]) were significantly higher in SLE patients, notably those with active disease, than in HD (**Figures 1D and 1E**). Further, the frequency of such $CD61^+$ Treg aggregates significantly correlated with SLE disease activity, as assessed by the SLE disease activity index (SLEDAI) (**figure 1F**). The specificity of platelet-cell aggregates was confirmed using CD41 together CD61 (**figures S1H-I**). Moreover, we confirmed that platelet/Treg aggregates were positive for P-selectin (CD62P, **figure S1J).** Of note, the frequency of platelet/T-effector aggregates was not significantly different between SLE and HD (**figure 1G**) and did not correlate with the SLEDAI (data not shown). Finally, platelet Tregs physical interaction was further confirmed by staining freshly sorted healthy donors' CD4+ T cells with CD41 (red) and FoxP3 (green) **(figure 1H**). Together, these results suggest that in active SLE patients, activated (P-selectin-expressing) platelets are responsible for a specific platelet/Treg interaction most likely *via* P-selectin/PSGL1 interaction.

Platelets block Tregs and Tfr suppressive functions through P-selectin/PSGL-1 interaction

To investigate the consequences of platelet-Treg interaction, we conducted Treg suppressive assays in the presence or absence of autologous platelets. While the platelets did not directly impact Teff cell proliferation, they prevented the suppressive function of Tregs (**figure 2A and 2B**) in a dose-dependent manner (**figure 2C**), and at a platelet-Treg ratio as low as 5:1. To distinguish whether platelet-mediated Treg dysfunction was mediated through a soluble or membrane-bound factor, we separated

the supernatant (without quantifiable sP-selectin, data not shown) and membrane-bound factors (pellet) from thrombin-activated platelets by ultracentrifugation and added each fraction to the Treg-Teff co-culture. Only the pellet from activated platelets inhibited Treg suppressive functions (**figure S2A**). Interestingly, preincubating Tregs with an anti-PSGL1 blocking antibody prevented platelet-induced Treg dysfunction (**figure 2D**), suggesting that the PSGL-1/P-selectin interaction mediated the platelet-driven inhibition of Treg suppressive function.

To assess whether this effect was specific to the PSGL-1 axis, we repeated the Treg suppressive assays, replacing platelets with recombinant forms of the known PSGL-1 receptors, i.e. Platelet- (P-), Endothelial- (E-) or Leukocyte (L-) selectin. Platelet-induced Treg dysfunction was observed following culture with each of the recombinant selectins (**figure 2E**), with treatment with P-Selectin showing the strongest inhibition. P-selectin inhibited the suppressive function of Tregs in a dose-dependent manner (**figure 2F**), and this effect was prevented when Tregs were pre-treated with anti-PSGL-1 blocking antibody (**figure 2G)**. Importantly, Treg viability was not affected by P-selectin (**figure S2B**). Finally, we ruled out LPS contamination of recombinant P-selectin using a polymyxine assay (**data not shown**). Together, these results indicate that platelet-induced Treg dysfunction was mediated by the interaction between P-selectin expressed on platelets and PSGL-1 expressed on Tregs.

To investigate if selectins had a similar effect on Tfr cells, we cocultured autologous memory B cells, Tfh and Tfr cells (or Tregs) sorted from HD, in the presence of Staphylococcal Enterotoxin B (SEB). While no impact on B cells was observed in the absence of regulatory cells, P-selectin inhibited Tfr and Treg immunosuppressive functions with respect to B cell differentiation into $CD38^{high}$ plasmablasts (**figures 2H and I**) and IgG production (**Figure 2J**). These results suggest that P-selectin is also able to block the suppressive properties of Tfr cells. These data identify a novel function of selectins in disrupting the suppressive activities of Tregs and Tfr cells.

P-selectin induces Syk kinase phosphorylation and intracellular calcium release in Tregs

PSGL-1 engagement has previously been described to induce Erk phosphorylation in neutrophils *(18)* and Syk phosphorylation in T cells *(19)*. To address the intracellular signaling pathways activated by selectins in Tregs, we used Phosflow® on freshly sorted Tregs from a HD. We found that P-selectin induced Syk phosphorylation in a dose-dependent manner (**figures 3A and 3B**), and this was inhibited by pre-incubation of Tregs with an anti-PSGL1 blocking antibody or with a Syk-specific inhibitor used as a negative control (**figure 3B**). Consistent with a role for Syk in regulating Treg function, Syk inhibition prevented the P-selectin-induced Treg dysfunction in immunosuppressive assays (**figure 3C**). In fresh blood samples from active SLE patients, $FOXP3^+$ Tregs aggregating with platelets ($CD61^+$ $FoxP3^+$ Tregs) had increased pSYK levels compared to $CD61^-$ Tregs (**figures 3D and 3E**). In contrast, we did not detect differences in pSYK levels between $FoxP3^-$ Teff cells alone or those that aggregate with platelets (**figure 3F**), likely due to the absence of CD15s. No significant difference was observed in Erk phosphorylation in Tregs in the presence of P-selectin stimulation (**figure S3A**). In addition, pre-incubating Tregs with different levels of P-selectin did not alter STAT5 phosphorylation in response to IL-2, suggesting that P-selectin did not affect the IL-2 axis in Tregs (**figure S3B**).

Phosphorylation-driven Syk activation leads to its interaction with and activation of phospholipase C-γ1 (PLC-γ1), triggering a cytosolic calcium ($[Ca^{2+}]_{cyt}$) signal *(20)*.

To measure $[Ca^{2+}]_{cyt}$ in Tregs, we conducted single-cell cytosolic calcium imaging on freshly isolated HD Tregs. Upon P-selectin exposure, cytosolic calcium concentration dramatically increased in Tregs (**figures 3G and 3H**), but not in B lymphocytes devoid of PSGL1 expression, or in Teff cells expressing low levels of fucosylated PSGL-1 (**figures S3C and S3D**). The pre-incubation of Tregs with anti-PSGL1 blocking antibody or Syk inhibitor prevented the P-selectin-mediated $[Ca^{2+}]_{cyt}$ increases (**figures 3G and 3H**). Collectively, these data identified the Syk/PLC-γ1 as key downstream mediators of selectin-induced Treg dysfunction, and that this pathway is activated in Tregs that aggregate with platelets in SLE patients.

Selectins trigger Treg dysfunction through inhibition of the TGF-beta pathway

To investigate the pathways altered downstream of Syk/PLC-γ1/calcium signaling in Tregs upon P-selectin exposure, we cultured freshly sorted human Tregs from HD for 8 hours with P-selectin and then investigated the transcriptional changes in the cells by microarray analysis. 3408 transcripts were significantly downregulated and 2229 were upregulated (|fold change| > 1.5 and p-value < 0.05) in response to P-selectin exposure (**Supplementary file 4 for the list of transcripts**). Interestingly, Treg-specific transcripts were downregulated including *FOXP3*, *IKZF2* (Helios), and *BCL11B* (**figure 4A**), while there was a moderate increase in transcripts of pro-inflammatory genes such as *IL17A*, *CCL4* and *IL18*. Gene set enrichment analysis identified that the TGF-beta signaling pathway was enriched in untreated versus P-selectin-treated Tregs, suggesting a selectin-dependent impairment of the TGF-beta axis in Tregs (**figure 4B**). Indeed, the transcripts of TGF-beta (*TGFB1*), its chaperone protein GARP (*LRRC32*) and the downstream transcription factor *SMAD3* were significantly downregulated in Tregs upon exposure to P-selectin (**figure 4A**).

Using qRT-PCR, we confirmed the downregulation of *TGFB1* and *LRRC32* mRNA in Tregs exposed to P-selectin ($p<0.01$, **figure 4C**). Next, to evaluate the impact of P-selectin treatment on Tregs at the protein level, we cultured HD Tregs for 48 hours with or without P-selectin and assessed GARP surface expression on Tregs using flow cytometry. We observed that P-selectin treatment was associated with decreased GARP expression on Tregs in a dose-dependent manner (**figures 4D and 4E**). Pre-incubation of Tregs with anti-PSGL-1 or Syk inhibitor restored GARP expression (**figure 4E**). GARP is a chaperone protein essential for the processing and release of active (free) TGF-beta by Tregs *(21)*. Therefore, we measured free TGF-beta levels in Tregs culture supernatants and found that P-selectin significantly decreased TGF-beta secretion by Tregs (**figure 4F),** without significantly altering the levels of IL-4, IL-10 or IL-17A (data not shown). To support platelet's role in P-selectin-mediated Treg dysfunction, we cultured Tregs with non-activated or ADP-activated platelets. ADP-activated platelets (and at a lesser extent non-activated platelets) significantly decrease FoxP3, Helios and GARP expression in a PSGL-1-dependent manner (**figure S4A**). Interestingly, TNF-alpha-activated endothelial cells (expressing P-selectin) failed to induce the same effect on Tregs (**figure S4B**) because of platelet-derived TGF-beta (data not shown).

In accordance with our microarray analysis, the Treg-specific transcription factors FoxP3 and Helios were significantly downregulated at the mRNA (**figure 4C**) and protein (**figures 4G-I**) levels after P-selectin exposure. FoxP3 and Helios downregulation was blocked by treating Tregs with the either anti-PSGL1 blocking antibody or Syk inhibitor (**figures 4H and 4I**). Importantly, upon P-selectin exposure, supplementing Tregs with TGF-beta rescued FoxP3 and Helios expression, supporting the importance of the TGF-beta pathway in Treg function and maintenance (**figure**

S4C). In contrast, Treg surface expression of CD25, CTLA4 and GITR were not modified by P-selectin exposure (**figure S4D**). Moreover, P-selectin did not induce Th17 gene set expression, and Tregs cultured with P-selectin for 48 hours did not upregulate RORγt or IL17 at the protein level (**figure S4E**). Exposure to P-selectin did not affect the expression of Tbet, GATA3 or RORγt in primary Th1, Th2 or Th17 cells respectively (**figure S4F**), further demonstrating the specificity of the selectin/PSGL-1 axis in Tregs. Collectively, these data suggest that P-selectin leads to specific Treg dysfunction by inhibiting the TGF-beta pathway and decreasing both FoxP3 and Helios expression.

P- and E- selectins are upregulated in SLE patients

To confirm the role of selectins in human SLE pathogenesis, we evaluated soluble selectin concentrations and selectin-bound microparticles in patients with SLE. Platelet-free plasma was isolated from fresh blood samples through a rigorous preanalytical protocol to avoid non-specific platelet activation as described in the *methods* section.

We subsequently measured levels of soluble selectins by ELISA. Consistent with previous findings, we found that soluble selectins (roughly the size of albumin) are lost in the urine in case of proteinuria seen in active glomerulonephritis *(22)*. Urinary P-selectin levels correlated with albuminuria (**figure S5A**), while blood P-selectin concentrations inversely correlated with albuminemia (reflecting urinary protein loss; **figure S5B**), suggesting urinary loss of P-selectin during active glomerulonephritis. For these reasons, we excluded patients with active renal disease (n = 6) from soluble selectin analysis. P- and E-selectin levels were increased in patients with active SLE compared to HD and quiescent SLE patients (**figure 5A**), and they significantly correlated with SLE disease activity (P-selectin: $r = 0.35$, $p = 0.005$; E-selectin: $r = 0.41$, $p < 0.001$; **figure 5B**), while this was not observed for L-selectin.

Next, we studied circulating levels of platelet- (PMP), endothelial- (EMP) and granulocyte-derived microparticles (GMP) in patient platelet-free plasma, as well as the expression of P-, E- or L-selectin, respectively by flow cytometry **(figure S5C and S5D)**. In line with a recent study (Mobarrez et al., Sci Rep 2016), we found that patients with active SLE had a moderate but significant increase in PMPs when compared to HD (**figure 5C**). Interestingly, while MP counts did not correlate with disease activity (**figure 5E**), selectin-positive MPs were markedly higher in active SLE patients (**figure 5D**) and correlated with disease activity as assessed by the SLEDAI (**figure 5F**). Precisely, we found a significant correlation between P-selectin$^+$ PMPs/E-selectin$^+$ EMPs and the SLEDAI (Psel$^+$ PMPs : $r = 0.52$, $p < 0.0001$; Esel$^+$ EMPs : $r = 0.42$, $p < 0.001$; **figure 5F**). In contrast to soluble P-selectin levels (**figure S5E**, left panel), P-selectin+ PMPs were significantly elevated in SLE with active renal disease compared to HD (**figure S5E,** right panel). Altogether, these data establish that active SLE patients are characterized by increased expression of selectins both in their soluble and microparticle-bound forms.

P-selectin blockade ameliorates SLE pathogenesis in lupus-prone mice

Finally, we investigated whether blocking P-selectin in a lupus-prone mouse model could alleviate cardinal features of the disease. To address this question, we first confirmed whether PSGL-1 expression in mice recapitulates that found in humans. We analyzed PSGL-1 expression on Tregs and Teff cells from C57BL/6 wild-type (WT) mice and observed that it was higher on FoxP3$^+$ Tregs compared to effector T cells. (**figure 6A-B**). Then, we explored whether P-selectin induced a calcium response in

Tregs ($CD4^+CD25^+$ T cells) and Teff cells ($CD4^+CD25^-$ T cells) sorted from the spleen of WT mice. As with human Tregs, recombinant mouse P-selectin induced a strong cytosolic calcium increase in mouse Tregs but not in Teff cells (**figures 6C and 6D**). Finally, we investigated whether P-selectin alters mouse Treg phenotype and function. We purified naïve CD4+ T cells from the spleen of WT mice, labelled them with CFSE and cultured them under different polarizing conditions to induce differentiation towards Th1, Th2, Th17 or Treg lineages. P-selectin treatment was associated with a specific decrease in FoxP3 expression in Tregs, with no impact on the lineage-specific expression of Tbet, GATA3, or RORgt in other subpopulations or overall proliferation of cells detected (**figures 6E and 6F**). Importantly, supplement of the cultures with increasing levels of TGF-beta was able to rescue FoxP3 expression in Tregs exposed to P-selectin (**figure S6A**). Furthermore, P-selectin induced a PSGL-1-dependent intra-cellular calcium signal in Tregs (**figure S6B**), but not in Teff (**figure S6C**). Together, these results confirmed that a P-selectin-binding PSGL1 is ~~highly~~ expressed on murine Tregs but not on Teff, and that selectins negatively impact murine Tregs and the TGF-beta pathway in the same manner as in humans. We further studied the relevance of selectins in a murine model of SLE by using mice deficient for DNase1L3. These mice develop all the major clinical features of human SLE including DNA autoreactivity and glomerulonephritis *(23)*. Furthermore, SLE pathogenesis in this model was shown to depend on the aberrant accumulation of self-DNA on MPs *(23)*. Therefore, we measured the circulatory levels of PMPs and their expression of P-selectin. While the total number of PMPs did not change **(figure S6D left panel**), the levels of P-selectin$^+$ PMPs were significantly higher in the plasma of *Dnase1l3*$^{-/-}$ knockout (KO) mice compared to WT ones **(figure S6D right panel**).

Together, these observations prompted us to test the therapeutic potential of P-selectin blocking antibody in *Dnase1l3* KO, lupus-prone mice. We treated 30 week-old KO mice with an anti-P-selectin monoclonal antibody (mAb), or with a control mAb during 10 consecutive weeks with 3 treatments/week. As expected, the anti-P-selectin antibody blocked P-selectin-induced calcium signaling in *ex-vivo* treated Tregs (**Figure S6E**) and reduced circulatory levels of P-selectin+ PMPs (**Figure S6F**). 30 week-old KO mice display elevated levels of anti-dsDNA autoantibodies compared to WT animals, and while these titers continued to increase over time in animals treated with control antibody, anti-P-selectin antibody prevented this increase (**figure 7A**), without altering total IgG levels (**figure S7A**). SLE development in KO animals is accompanied by a loss of marginal zone B cells (MZB), which was also partially rescued by anti-P-selectin antibody (**figures S7B and S7C),** while other B cell subpopulations were not significantly modified (**figures S7D and S7E**). The accumulation of autoreactive antibodies together with C3 complement causes their deposition in the kidney glomeruli of KO mice (**figure 7B, lower panels**) and ultimately leads to the development of glomerulonephritis manifested by enlarged glomeruli, mesangial proliferation and sometimes glomerular thrombosis (**figure 7D middle panel**). Finally, after 10 weeks of anti-P-selectin treatment IgG/C3 deposition in the kidney was reduced (**figure 7C),** and the overall pathology was significantly improved (**figure 7D, right panel and figure 7E)**. These results show that P-selectin blockade significantly ameliorates pathogenesis in a murine model of SLE.

Discussion:

In this study we identified selectins, in particular P-selectin, as a new potential therapeutic target in SLE. Indeed, we observed that selectins produced by activated platelets (P-selectin), granulocytes (L-selectin), and endothelial cells (E-selectin) specifically block the immunosuppressive properties of Tregs, without affecting effector T cells. Selectins induced a Syk-dependent calcium increase, which inhibited TGF-beta and led to reduced expression of Foxp3. Assessment of circulating levels of selectins, selectin-bound microparticles, and platelet/Treg aggregates revealed that this P-selectin pathogenic pathway was active in SLE patients. Finally, we observed a similar effect of P-selectin on murine Tregs, and targeting P-selectin by a blocking mAb in a mouse model of SLE improved cardinal disease parameters, including anti-DNA antibody levels and kidney pathology.

Tregs are vital to the preservation of immune tolerance and prevention of exacerbated immune responses that lead to autoimmunity. Foxp3$^+$ Tregs are characterized by their constitutive and high expression of CD25 (IL-2 receptor a chain) and the co-inhibitory molecule CTLA-4. Tregs quickly sense and consume IL-2 produced by effector T cells to prevent their activation *(24)*. Foxp3$^+$ Tregs use additional suppressive molecules including IL-10, TGF-beta, IL-35, TIGIT, CD39, and CD73 to mediate their inhibitory functions. In our study, platelet- (and not endothelium-) derived P-selectin was responsible for an inhibition of the TGF-beta pathway, as well as for a moderate downregulation of FoxP3 and Helios (figure S4A-B). While the downregulation of FoxP3/Helios was moderate, several other studies demonstrated impaired Tregs functions with moderate FoxP3 modulation *(6, 25)*. Additionally, although platelets may be a source of TGF-beta, we found a the net effect was a inhibition of Tregs functions *(26)*. In the context of SLE, studies have led to contradictory results regarding Treg numbers *(27)* and/or function *(28)*. Nevertheless, an impairment in Treg function is likely since treatment with low-dose IL-2, which restores the Treg compartment, improves the disease in humans *(29, 30)*. However, the exact mechanisms involved in Treg dysfunction in SLE remained largely unknown. Our data established selectins as inhibitory factors that selectively target Tregs and Tfr cells. Binding of the selectin family on PSGL-1 depends on post-translational modifications such as fucosylation, which inserts the Sialyl Lewis X motif (sLe^x). We observed that CD15s, which is specifically expressed by Tregs and Tfr cells, was associated with the ability of PSGL-1 to induce intracellular signals in response to selectin, leading to alterated Treg functions. Interestingly, CD15s^{high} Tregs have been described as terminally differentiated and mostly immunosuppressive Tregs *(17)*.

Selectins are upregulated in a wide range of inflammatory disorders, and their function was believed to be limited to chemotaxis *(10)*. Several SLE mouse models show elevated levels of P-selectin in the serum and affected tissues *(22, 31)*. The role of the selectin/PSGL-1 pathway in the context of immune tolerance is poorly understood. Tinoco *et al.* demonstrated that the deletion of PSGL-1 in mice was associated with an increased virus-specific or tumor-specific CD8$^+$ T cell response and induced an uncontrolled autoimmune response that quickly became fatal *(16)*. However, as this effect was mainly driven by CD8$^+$ T cells that do not express fucosylated PSGL-1 and treatment with P-, E- or L-selectin did not have an impact on the antiviral response, PSGL-1 likely mediated its effects through a selectin-

independent mechanism in this model. These results were recently explained by Johnston et al who showed that PSGL-1 is a ligand of a checkpoint molecule, the V-domain Immunoglobulin Suppressor of T cell Activation (VISTA) in acidic condition such as the tumor microenvironment *(15)*. Another work suggested that PSGL-1 engagement with P-selectin induced a tolerogenic phenotype in immature DCs *in vitro (32)*. Therefore, it appears that PSGL-1 exerts multiple functions in inflammation in a cell- and environment-specific manner, beyond its initial role described in selectin-mediated rolling and diapedesis. In addition to blocking Treg function, P-selectin was also shown to both trigger NETosis in mouse neutrophils *(33)* and activate monocytes *(34)*, two important features of SLE pathogenesis. Whether these mechanisms (e.g. platelet-dependent activation of monocytes and neutrophils) contribute to SLE remains unclear. However, it is tempting to speculate that P-selectin-targeting therapies could impact multiple immune pathways involved in SLE pathogenesis.

Platelets are one of the main sources of circulating P-selectin, and besides their well-established role in hemostatic functions, they are increasingly recognized as important players in inflammation *(35–37)*. Pioneering studies from Boilard *et al.* and our group have established a role for platelets in the amplification of inflammation by microparticle production in rheumatoid arthritis and aggregation to plasmacytoid dendritic cells in SLE *(9, 38)*. Very recently, Han and colleagues have shown that platelet interacted with monocytes through P-selectin/PSGL-1 and induced an antigen presenting cell phenotype with a direct relevance on the immune response in vivo in mice *(39)*. Importantly, immune cells and platelets may interact through several other components such as CD40-CD40L, SLAMF1 or GPIb/Mac1 *(9, 40, 41)*. Furthermore, platelets have been implicated in many inflammatory disorders including multiple sclerosis, systemic sclerosis, Crohn's disease *(37, 42)*, but also in cancer where they subvert T cell immunity via the TGF-beta axis *(43)*. While our results establish a new role for platelets in SLE, it is likely that the described P-selectin-mediated pathogenic pathway operates in other autoimmune diseases. In the context of SLE, epidemiologic studies revealed that platelet activation correlated with disease severity, occurrence of thrombosis, premature atherosclerosis, and long-term mortality *(8)*.

Premature atherosclerosis represents the first cause of death in SLE patients, and current immunosuppressive treatments fail to control its progression *(44)*. While traditional cardiovascular risk factors may partially be involved, the precise mechanisms leading to this accelerated atherosclerosis in SLE patients remain poorly understood *(45)*. The protective role of Tregs in atherosclerosis was previously characterized *(46)*, and elevated P-selectin levels have been widely associated with atherosclerosis progression and myocardial infarction in humans *(11)*, with causative links demonstrated in mouse models *(47)*. Together with our study these observations further indicate that P-selectin blockade could be an innovative treatment in SLE, targeting both the immune system dysregulation and the accelerated atherosclerosis. Notably, crizanlizumab, a human anti-P-selectin antibody has been developed and tested in sickle-cell disease, a haemoglobin disease characterized by red blood cell/platelet aggregation and small vessel thrombosis. This treatment has shown to be efficient in terms of vaso-occlusive crisis without safety warnings, paving the way for trials in other indications such as SLE *(48)*.

In conclusion, we describe a new pathologic pathway in SLE, where activated platelets ~~and endothelium~~ interact with Tregs to block their immunosuppressive

functions. Blocking P-selectin improved a murine model of SLE, supporting it as a potential therapeutic target for future clinical trials.

Materials and methods:

Human Samples. Healthy donor samples were obtained from the French National Blood bank (Etablissement Français du Sang). SLE patients were recruited in the rheumatology, nephrology and internal medicine departments of Bordeaux University Hospital. Patients were diagnosed with systemic lupus erythematosus using the 2012 SLICC SLE diagnosis criteria (Petri et al., arthritis, 2012). Oral and written consent were obtained from patients before samples (blood and/or urine) were retrieved. Our research protocol (MICROLUPS) conforms to French and European Ethics standards and was reviewed and approved by an independent ethical committee (authorization number 2018-A00599-46). The MICROLUPS research protocol was registered on *clinicaltrials.gov* (NCT03575156).

Phenotyping of blood cells. 200µL of fresh whole blood was stained with antibodies recognizing lymphocyte markers (see supplementary table 1). After 15 minutes of incubation at room temperature, red blood cells were lysed using 3mL of ACK buffer (150mM NH4Cl, 10mM KHCO3, 1mM EDTA2Na) for 25 minutes then washed with PBS. In order to study rare subpopulations (e.g., Tfr), PBMCs were isolated using Ficoll-Paque, and 10^7 PBMCs were stained for 15 minutes before washing and cytometer analysis.

Blood cell isolation. PBMCs were retrieved from healthy donors or patients using Ficoll-Paque separation medium (Eurobio, France®). To sort Tregs and Teff, PBMCs were pre-sorted using CD4-microbeads with Magnetic-Activated Cell Sorting (Miltenyi©) following the manufacturer's instructions. CD4-sorted cells were then stained with CD4-PE-Cy7 (Beckman-Coulter©), CD25-PE-Cy5 (Beckman-Coulter©) and CD127-PE (Beckman-Coulter©). The $CD4^+$ Cells were subsequently sorted using FACS Aria 2-Blue 6-Violet 3-Red 5-YelGr, 2 UV laser configuration (BD Biosciences©) in flow cabinet. T regulatory lymphocytes (Tregs) were identified as $CD4^+/CD25^{high}/CD127^{dim}$ and T-effector (Teff) lymphocytes as $CD4^+/CD25^-/CD127^+$. Subset purity was 95% or higher. T follicular regulatory cells (Tfr) were sorted as $CD4^+/CD25^{high}/CD127^{dim}/CXCR5^+$ cells and T follicular helper (Tfh) cells as $CD4^+/CD25^-/CD127^+/CXCR5^+$.
Magnetically enriched $CD19^+$ cells were sorted using ARIA FACS. Memory B cells were sorted as $CD19^+CD27^+IgD^-$ and naïve B cells were $CD19^+CD27^-IgD^+$.
Platelets were isolated from platelet-rich plasma (PRP), which was generated from freshly drawn whole blood samples by 20 minutes centrifugation 180 x g, with no brake applied. Prostaglandin E1 (1µM). was added to the PRP to prevent excessive platelet activation during sample preparation. Platelets were pelleted by centrifugation at 890 x g, without brake, for 10 minutes, and re-solubilized in Tyrode's buffer (NaCl 0.134M, KcL 2.9mM, NaH2PO4 0.34mM, NaHCO 12m, HEPES 20mM, MgCl2 1mM, Glucose 5mM, BSA 0.5%). Before use, platelets were counted using a Beckman Coulter© ACT diff analyzer.

Immunofluorescence of platelet/Treg aggregates. Fresh healthy human PBMCs were magnetically sorted (Myltenyi©) and placed on a slide. After centrifugation. (300xg, 5 minutes), the slides were stained with rabbit anti-FoxP3 (Abcam© clone SP97, 1/50) and mouse CD41 (Abcam© clone M148, 1/400). Goat Anti-mouse-AF-568 and goat anti-Rabbit-FITC polyclonal antibodies were used at 1/500 for revelation (see supplementary table 3 for references). Slides were acquired with a Leica DM5000.

Treg immunosuppressive assay. After sorting, Teffs were stained with carboxyfluorescein succinimidyl ester (CFSE) 2mM to monitor proliferation. 50,000 Tregs / well were plated in a 96-well plate coated with anti-CD3 (UHT1, Beckman Coulter©, 1 µg/mL). When used, anti-PSGL1 antibody 1/200 (clone KPL1) or Syk inhibitor 1µM (Cayman Chemicals©, Ref 622387-85-3) were added to the Tregs and incubated at 37°C for 30 minutes. Platelets or selectins (200pg/mL) were subsequently added and incubated at 37°C for 45 minutes. In experiments involving selectins, the cells were subsequently washed and supernatant containing inhibitor and selectin removed after centrifugation. After washing, Teffs were added at a 1:1 ratio with Tregs and an anti-CD28 antibody was added (clone CD28.2, Beckman coulter©, 3 µg/mL). As a control, Teff cells were also cultured alone with or without platelets and/or selectin to assess the potential effect on proliferation. Co-cultures were incubated 4 to 6 days then stained with DAPI and CD4 to assess CFSE fluorescence dilution in viable cells using a BD CantoII® cytometer.

Tfr immunosuppressive assays. In a 96-well plate, 30,000 freshly-sorted B memory cells were cultured at a 1:1:1 ratio with autologous Tfh cells and Tfr or Treg cells. Cells were cultured with SEB (1µg/mL) for 7 days at 37°C, with or without P-selectin (200pg/mL). Supernatants were subsequently frozen, and the cell pellets analyzed by flow cytometry (see supplementary table 1 for antibodies). Plasmablasts were defined as live $CD4^{-}CD19^{+}CD27^{high}CD38^{high}$ cells. IgG measurements from supernatants were conducted using the ELISA Human IgG quantification kit (Bethyl laboratories©, cat. E80-104) per the manufacturer's instruction.

Calcium signaling assay. Single-cell cytosolic calcium imaging was performed using the fluorescent calcium dye cali-520 (AAT Bioquest, CA, USA). Glass coverslips were mounted in a Attofluor cell chamber (Thermo Fisher Scientific, Saint Herblain, France) positioned on the stage of an inverted epifluorescence microscope (IX70, Olympus) equipped with an ×40 UApo/340- 1.15W objective. $5x10^5$ Tregs or Teff were loaded with cali-520 (1µM) at room temperature (20–25 °C) in Hank's Balanced Salt Solution (HBSS, 2mM CaCl2, pH 7.25) for 30 minutes. Cali-520 exhibits limited compartmentalization in intracellular stores and is resistant to leakage. The cells were rinsed with HBSS and incubated in the absence of the Ca^{2+} probe for 15min to complete de-esterification of the dye. Cali-520 was excited at 485+/− 22nm, and images were captured at 530+/− 30nm at constant 10-s intervals, at 12-bit resolution, by a fast-scan camera (CoolSNAP fx Monochrome, Photometrics). All images were background-subtracted. Regions of interest corresponding to cells recorded were drawn to analyze the fluorescence signal. Imaging was controlled by Universal Imaging software, including Metafluor and Metamorph. Fluorescence intensity changes were normalized to the initial fluorescence value F0 and expressed as F/F0 (relative $[Ca^{2+}]_{cyt}$). One field was acquired from each coverslip, and the data pooled from six independent coverslips on three different days. The calcium traces were quantified by determining the area under the curve (AUC) using OriginPro 7.5 software (Origin Lab).

Microarray analysis and RT-qPCR. 5x10^5 Tregs were incubated at 37°C on a CD3-coated plate (1µg/mL) during 8 hours with or without recombinant human P-selectine (R&D systems) at 200pg/mL. After incubation, cells were washed with PBS and lysed using QIAGEN RNeasy micro kit plus®. RNA was subsequently extracted using the manufacturer's instructions. RNA purity was assessed by Agilent Total RNA nano Series II asay with RIN > 8.0. Transcriptomic assay was performed using a Nugen Chip at the GENOM'IC platform, Institut Cochin, Paris. Analysis was conducted using R software (R project©). Differential expression of transcripts was computed on paired samples (each donors' Tregs), untreated or treated with P-selectin, using limma paired sample analysis. Reverse transcriptase reactions were conducted on 200ng of RNA using Promega© GOSCRIPT RT protocol®. qPCR reaction (Promega© SYBR GoTaq®) was conducted using a CFX384 C1000Touch® thermal cycler (Bio-Rad©) on 3ng of complementary DNA using specific primers from Sigma-Aldrich© (suppl table XX). Stable housekeeping genes was selected (EEF1A1). Differential expressions were calculated using the threshold cycle (Ct) and the comparative Ct method (ΔΔCt) for relative quantification.

Study of phosphorylated proteins. 10^5 purified Tregs were plated on a non-coated 96-well plate. After 4 hours of culture, 37°C pre-warmed medium containing the stimulus (P-selectin or IL-2) or control medium was added to the selected wells, and the plate was incubated at 37°C for 5 to 30 minutes. After incubation, BD Cytofix® was added for fixation. The BD Perm III buffer® was used for permeabilization following the manufacturer's instructions (BD phosflow®). Staining was conducted on ice for 1 hour (see supplementary table for antibodies and dilution).

Culture of Tregs and FoxP3 phenotyping. 10^5 freshly purified Tregs were plated on a CD3-coated 96-well plate. Tregs were incubated with anti-PSGL1 antibody (1/200) or Syk inhibitor (1 µM) during 30 minutes before adding the P-selectin. After 48 hours of incubation, the cells were fixed and permeabilized using EBioscience© FoxP3 staining kit following the manufacturer's instructions.

Platelet-free plasma isolation. Preanalytics was standardized for all samples to prevent non-specific platelet activation and microparticle production after blood puncture. Venipuncture was performed on resting patients, without tourniquet, using a 21- or 19-gauge needle. Samples were collected in 7mL EDTA-coated tubes (BD Vacutainer®) after a 3mL blood purge. Immediately after collection the tube was inverted once to prevent coagulation. The samples were kept vertical on a tube holder and were transferred to the lab for processing in less than 2 hours after blood puncture. Platelet-free plasma (PFP) was produced by two sequential 15-minute centrifugations at 3500 x g without brake. After each centrifugation, two-thirds of the supernatant was retrieved and placed in a new tube. PFP samples were subsequently aliquoted and stored at -80°C until further analysis.

ELISA and cytokine measurement. Human P-, E- and L-selectins were measured using ELISA (R&D systems, DuoSet ELISA) on PFP samples following the manufacturer's instructions. Free active TGF-beta was measured from Treg culture supernatants using cytometric bead assay (CustomPlex, Biolegends©) according to the manufacturer's protocol.

Microparticle analysis by flow cytometry. Absolute counts of subset-specific, circulating MPs were characterized by flow cytometry using the BD LSRFortessa™ X-20 cell analyzer. PFP aliquots were thawed at room temperature and 10 µl of PFP was used for MP staining. MPs were stained in a total volume of 100µL of 0.22µm filtered PBS-BSA 0.5%, in BD Falcon Polystyrene round Bottom tubes for 2 hours in the dark at room temperature with titrated antibodies specific for different MP subsets (see supplementary table 1 for clones and dilutions). MPs derived from platelets (PMPs) were identified using anti-CD61-viogreen, MPs from endothelial cells (EMPs) by anti-CD31-APC and MPs from granulocytes (GMPs) by anti-CD66b-PE-Cy7. Selectin expression status on PMPs, EMPs and GMPs were identified by using respectively anti-CD62P-PE, anti-CD62E-PEvio770 and anti-CD62L-PE (see supplementary table 1 for dilution). After staining, MPs were diluted by adding 400 µL of staining buffer. 50 µl of labeled and diluted MP suspensions were transferred into BD Trucount™ Tubes (BD Bioscience®) for absolute quantification (MP counts/mL) of PMPs, EMPs and GMPs. The overall number of MPs was defined as the result of the sum of the absolute count of each MP subset (PMPs and EMPs). Forward scatter (FSC) and side scatter (SSC) were adjusted to logarithmic gain. A standardized method for determining the MP gate was established using fluorescent beads of different sizes (Megamix-Plus SSC: 0.16, 0.20, 0,24 and 0,5 µm (BioCytex, Marseille®)). To reduce background noise, we adopted a fluorescent-triggering strategy as described by Arraud et al *(49)*. Briefly, fluorescence signal from Viogreen, APC or PC-7 were used to trigger detection of MPs labeled with anti-CD61-viogreen (PMPs), anti-CD31-APC (EMPs) or anti-CD66b-PE-Cy7, respectively. As a negative control for labeled-MPs, PFP samples were prepared as above and then treated with 0.5% Triton X-100 solution in order to disrupt vesicles (**figure S5D**). PMPs were considered as $CD61^+$ events in the MP gate, which were removed by Triton treatment. Similar gates were used for EMPs and GMPs using CD31 and CD66b, respectively.

For measurement of mouse PMPs, the PFP was isolated following the same centrifugation protocol as in human. Before staining, 100µL of PFP diluted with 400µL of filtered PBS-BSA 0.5% was concentrated by centrifugation for 45 minutes at 21,000xg. After discarding 450µL of supernatant, 30µL of concentrated PFP was stained with CD61-FITC and CD62P-PE (see supplementary table 1). Staining was conducted in the dark for 2 hours before analysis. We used the same acquisition and gating strategy for mouse MPs as for human MPs. MPs were quantified using BD Trucount™ Tubes following the manufacturer's instructions.

Mice. CD57/BL6 mice WT and *Dnase1l3*-KO were generously provided by V. Sisirak. 30 week-old mice were treated with anti-P-selectin antibody (clone RMP-1, Biolegend©) or its isotype control (MOPC-173, Biolegend©), 0.1mg intraperitoneally, 3 times per week for 10 weeks. The treatment protocol was reviewed and approved by an external animal ethics committee (authorization number APAFiS #19915). At the end of treatment, mice were euthanized and peripheral blood, kidneys and spleen were harvested. PFP was made from a terminal blood sample in an Eppendorf containing 50µL of EDTA 0.5M. Sections from frozen or paraffin-embedded kidneys were analyzed by immunofluorescence or light microscopy, respectively. Kidney sections were stained with hematoxylin-eosin for morphological study by a blinded kidney pathologist (AV). A glomerular injury score was calculated based on glomerular enlargement (0-1), interstitial infiltration (0-1 scale), mesangial proliferation (0-4 scale), glomerular thrombosis (0-2) and fibrosis (0-2 scale). Immunofluorescence staining was conducted on 10µm kidney section using Goat F(ab') anti-mouse IgG-PE (e-

Bioscience©, ref 12-4010-82, 1/250) and a rat monoclonal anti-C3 IgG (clone 11H9, Abcam© ref 11862, 1/200) with a secondary Goat anti-rat IgG-AF488 (Invitrogen©, ref A11006, 1/1000). The mean fluorescence intensity of each fluorochrome was evaluated in 40 glomeruli for each mouse using ImageJ software.

Anti-dsDNA ELISA. Anti-dsDNA antibodies were measured using ELISA as previously described *(23)*. Briefly, 96-wells plates were pre-coated with poly-L-lysine (0.05 mg/mL) for 2 hours at room temperature and then coated with 0.1 mg/mL of calf thymus DNA (Sigma-Aldrich) overnight. Coated plates were then incubated with sera samples for 2 hours. After washing, the amount of bound IgG was measured with an alkaline phosphatase-conjugated goat anti-mouse IgG antibody (1/5000, Jackson Immunoresearch). Anti-dsDNA IgG titers were determined using serial dilution of the serum from a positive animal as a standard, and expressed as units per volume.

Spleen phenotyping. Mouse spleens were mechanically crushed through a filter, and red blood cells were removed using ACK buffer *(23)*. The absolute count of live cells was obtained using BD Accuri® flow cytometer, and 10^7 cells were subjected to FcR-blocking followed by staining for phenotypic analysis (see supplementary table 1).

Mouse T lymphocyte differentiation. Naïve $CD62L^+$ $CD4^+$ T lymphocytes were purified using MACS (Miltenyi Biotec©; 130-104-453) from PBMCs isolated from spleens of CD57BL/6 wild type mice. 10^5 cells were plated in 96-well plate coated with anti-CD3 antibody (1µg/mL) with sCD28 (3 µg/mL) under polarizing conditions. For Tregs: TGF-beta (5ng/mL) and IL2 (20ng/mL); Th1: IL12 (10ng/mL) and IL2 (10ng/mL); Th2: IL4 (20ng/mL); Th17: IL6 (40ng/mL) and TGF-b (0.5ng/mL). After 6 days of culture, viable cells were stained with CD4 and their respective differentiation markers: CD25 and FoxP3 for Tregs, Tbet for Th1, GATA3 for Th2 and RORgt for Th17.

Statistics. Data are shown as individual values with the mean and standard deviation (except when specified otherwise). Quantitative data were compared using non-parametric Mann-Whitney test or non-parametric Kruskal-Wallis test with Dunn's correction for multiple testing of more than 2 groups (except when specified otherwise). Correlations were assessed using the non-parametric Spearman's correlation. Statistical significance was defined as p-value < 0.05. All statistical tests were conducted using GraphPad Prism® V7.

Data and code availability. Microarray results are available in the ArrayExpress repository (https://www.ebi.ac.uk/arrayexpress/).

Acknowledgements:

We would like to thank all sources of funding including the Fondation pour la Recherche Médicale (FRM), the Société Française de Rhumatologie (SFR), the Centre national de reference maladie auto-immune et systémique rares Est/Sud-ouest (RESO), the Bordeaux University Hospital and the Centre National de Recherche Scientifique (CNRS). V.S is supported by the IdEx program of the university of Bordeaux and the CLIP program from the cancer research institute. We thank all the patients involved in this study, as well as all the clinicians involved in their recruitment. We would like to thank Thomas Paz Del Soccoro for his help. Very warm thanks to Katie Sawai for her help concerning English editing.

Funding: All funding was provided by academic source or scientific foundations. [This work was not supported by any pharmaceutical companies.] → The authors declare no competing financial interests.

Ethical statement: All patients included in this study gave oral and written consent to participate. The study's protocol is in accordance with French and European Ethics standards and was approved by an independent ethical committee (number 2018-A00599-46). Healthy donors consented to take part in the study and were recruited through the French National Blood bank (Etablissement Français du Sang). All animal experiments were approved by an external animal ethics committee (authorisation number APAFiS #19915

Author contributions:

MSc performed most of the experiments, conducted the statistics analysis and designed the figures. V.G performed microparticle measurements from patients and HD. ID, IR and EM performed immunosuppressive assay experiments. PV conducted calcium measurement assays. JPG conducted the microarray analysis. NM and MSc conducted the mouse experiments with help from AG and AB. AV is a trained kidney pathologist who evaluated kidney histology. EL, LC, PD, JLP, JFV, TS, MET and CR were involved in the active recruitment of SLE patients. TB helped for the writing of the study protocol and submission to the ethics committee. VS provided mice and assistance with the related experiments and analysis of results. MSa, CCB and PL helped to design the experiments. PB and CR designed the study, oversaw all experiments and analysis of results. All authors critically reviewed and approved the manuscript before submission.

Figures and figure legends:

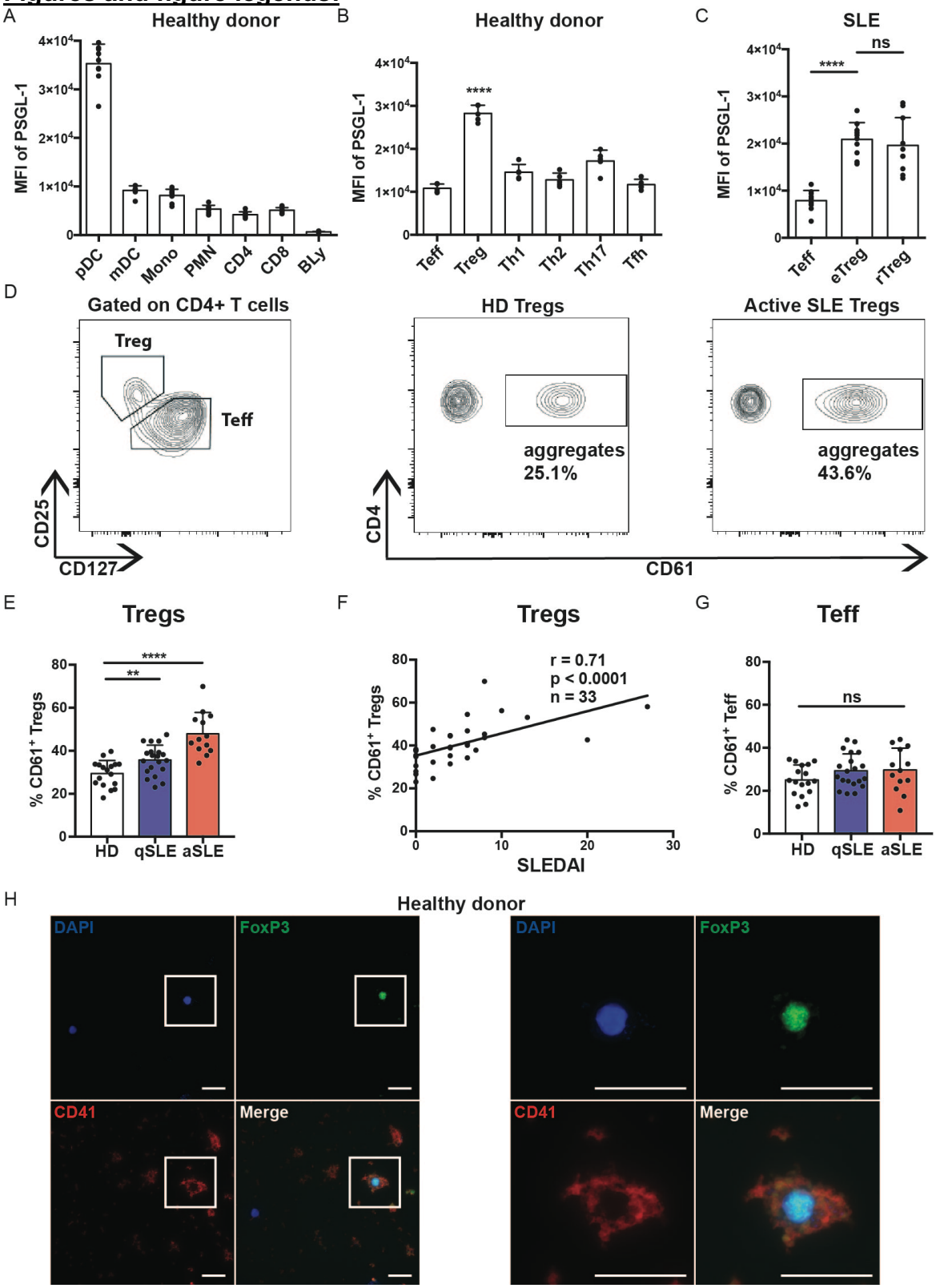

Figure 1: Tregs express high levels of PSGL-1 and interact with platelets in SLE patients

(A) Mean Fluorescence intensity (MFI) of PSGL-1 on circulating immune cells from healthy donors (n = 10).
(B) PSGL-1 MFI on T cell subsets from healthy donors (n = 5). ****, $p < 0.0001$ vs all other subpopulations using one-sided ANOVA with Holm-Sidak's correction for multiple tests.
(C) PSGL-1 MFI of $CD4^+CD25^-FoxP3^-$ T effector cells, resting ($CD45RA^+$) or effector ($CD45RA^-$) $CD4^+CD25^+FoxP3^+$ Tregs in patients with SLE (n=10).
(D) Representative gating of Treg-Teff/platelet aggregates from healthy donors and SLE patients.
(E) Cumulative results of Treg/platelets from HD and patients with quiescent SLE (qSLE, SLE disease activity index (SLEDAI) < 6, n = 20) or active SLE (aSLE, SLEDAI ≥6, n = 13) patients as shown in (D).
(F) Spearman's correlation between the percentage of Treg/platelet aggregates and the SLEDAI.
(G) Cumulative results of Teff/platelets in HD and qSLE and aSLE patients as show in (D).
(H) CD4+ T cells were magnetically sorted from an healthy donors and stained with DAPI, CD41 (red [secondary AF568], clone M148 Abcam©, 1/400) and FoxP3 (green [secondary FITC], clone SP97 Abcam©, 1/50). Scale bars indicate 20µm.

Dots represent the value of individual donors, columns represent the mean and error bars indicate S.D. **, $p < 0.01$; ****, $p < 0.0001$ using non-parametric Kruskal-Wallis test with Dunn's correction.

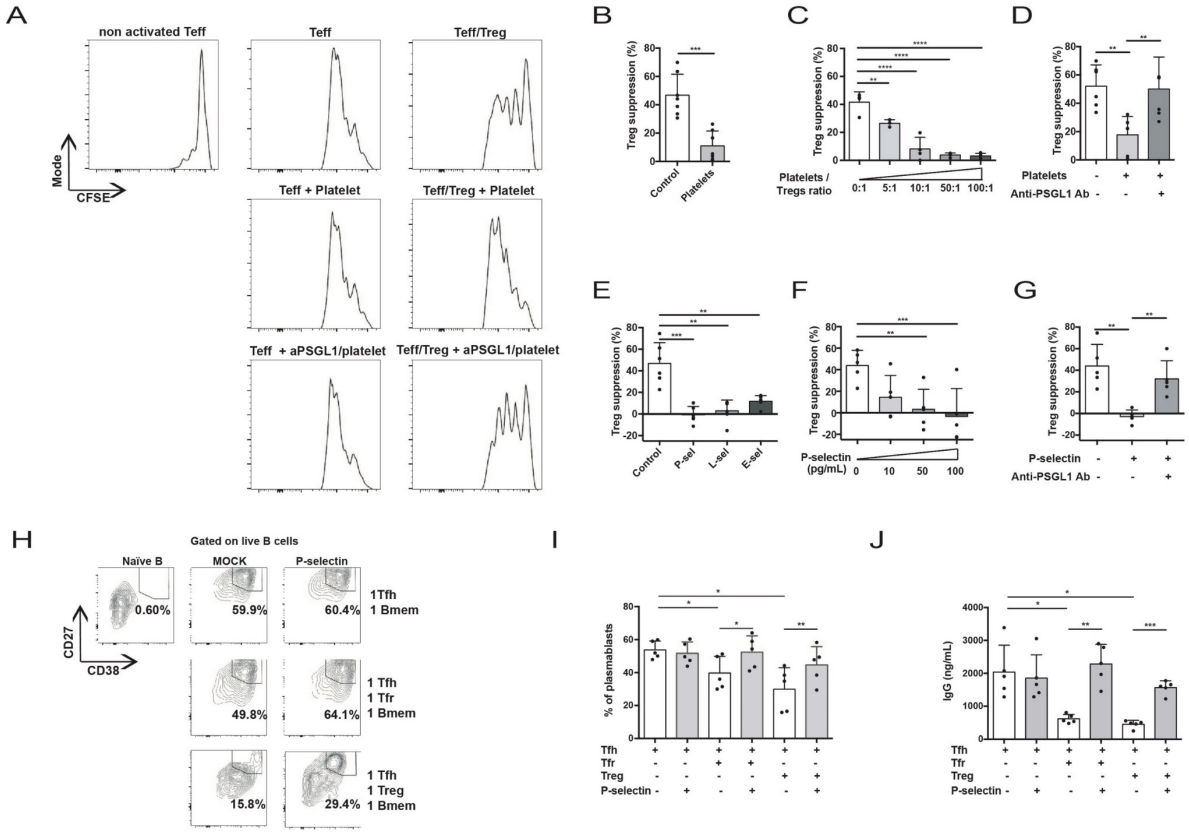

Figure 2: Platelets block Tregs suppressive capacities through the P-selectin/PSGL-1 axis

(A) Representative results of CFSE dilution in a Treg/Teff suppression assay with or without platelet (ratio Treg/platelet 1:100).

(B) Cumulative results of Treg/Teff suppression assay with or without platelets (ratio Treg/platelets 1:100; n = 7 independent experiments).

(C) Dose-response effect of platelets in the Treg/Teff suppression assays (n = 4).

(D) Effect of PSGL-1 blockade (clone KPL-1, dilution 1/200) on platelet-induced Treg dysfunction in suppression assay (n = 6).

(E) Effect of P- E- and L-selectin (200pg/mL) on Treg suppressive capacities in suppression assays (n = 6).

(F) Dose-response effect of P-selectin in the Treg/Teff suppression assay (n = 5).

(G) Effect of PSGL-1 blockade on P-selectin-induced Treg dysfunction in suppression assays (n = 5).

(H) Representative results of a B response suppression assay showing plasmablast ($CD27^{hi}CD38^{hi}$ B cells) differentiation with or without Tregs/Tfr and P-selectin (200pg/mL).

(I) Cumulative results of B response suppressions assays with or without P-selectin 200pg/mL (n = 5).

(J) IgG production measured by ELISA from the supernatant of the B response suppression assays (n = 5).

Dots represent the result of an independent experiment, the histograms represent the mean and the bars the S.D. *, $p < 0.05$; **, $p < 0.01$; ***, $p < 0.001$; ****, $p < 0.0001$ using one-sided ANOVA with Holm-Sidak's correction.

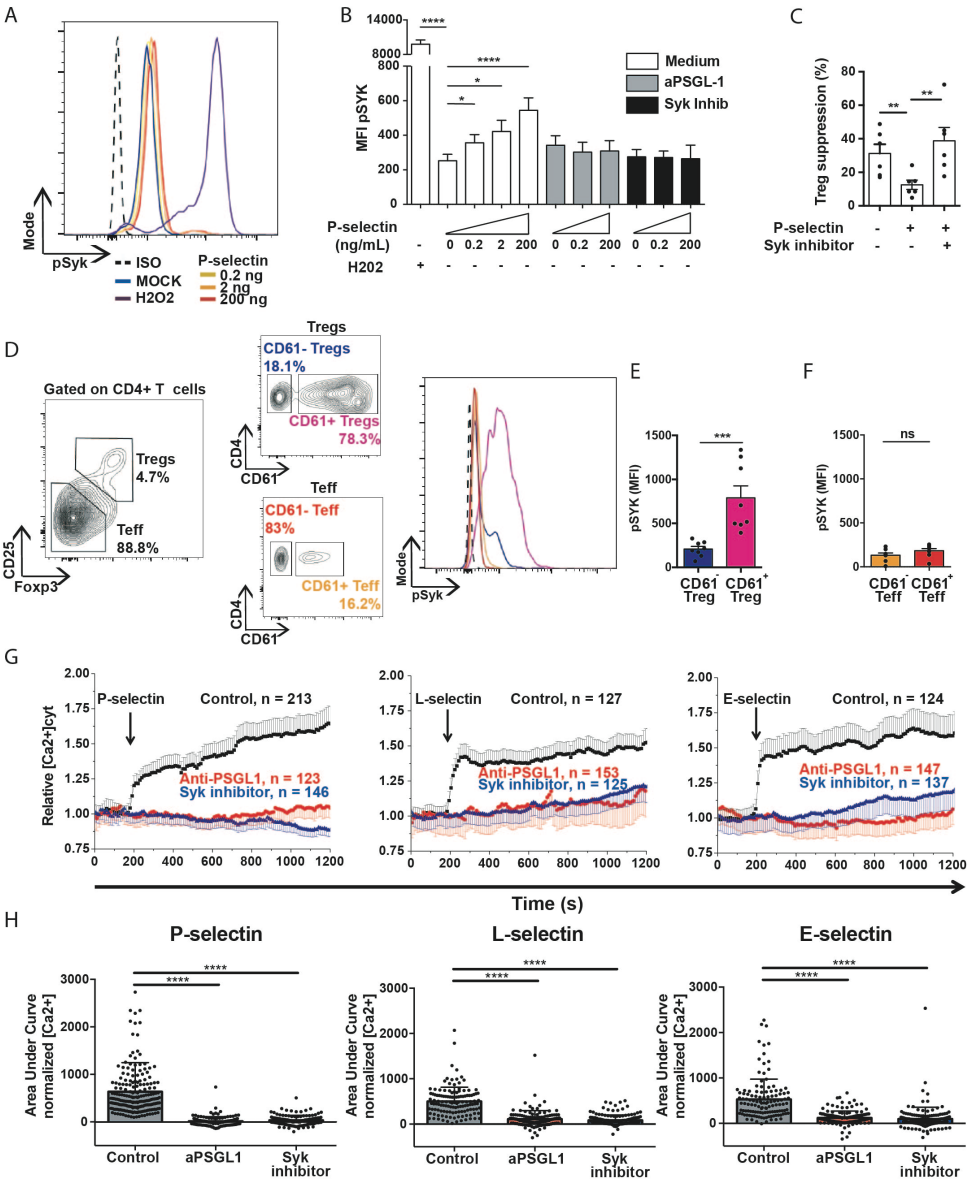

Figure 3: Selectins induce Syk/calcium signaling in Tregs *in vitro* and *ex vivo*

(A) Syk phosphorylation in Tregs exposed to P-selectin for 5 minutes using cytometry (Phosflow® protocole): representative results.

(B) Cumulative data of Syk phosphorylation in Tregs exposed to P-selectin for 5 minutes (n = 13 independent experiments, with or without 30 minutes preincubation with anti-PSGL1 antibody (1/200, n = 10) or a Syk inhibitor (1 µM, n = 4).

(C) Effect of Syk inhibitor (1 µM, 30 minutes) preincubation on Treg immunosuppressive functions by suppression assays (n = 6).

(D) Gating and representative pSYK expression of $CD25^{+}FoxP3^{+}$ Tregs and $CD25^{-}FoxP3^{-}$ Teff aggregating or not with platelets (CD61 expression) in fresh blood samples of active SLE patients (n = 6).

(E) Cumulative results of pSYK mean fluorescence intensity of $CD61^{+}$ and $CD61^{-}$ Tregs (n = 6). ***, $p < 0.001$ using bilateral unpaired Student t-test.

(F) Cumulative results of pSYK mean fluorescence intensity of $CD61^{+}$ and $CD61^{-}$ Teff (n = 6). NS, non-significant using bilateral unpaired Student t-test.

(G) Effects of P-selectin (left panel), L-selectin (middle panel), E-selectin (right panel) 200ng/mL on the intracytosolic calcium concentration ($[Ca^{2+}]_{cyt}$ using cal-520 as fluorescent calcium probe) of HD Tregs in control conditions (black), anti-PSGL1 antibody (1/200)-treated cells (red) and syk inhibitor (1µM)-treated cells (blue). Shown are representative results of 3 independent experiments from different HD, lines represent the mean value, bars the S.D. and n corresponds to the number of studied cells.
(H) Quantification of calcium responses using the determination of the area under curves (AUC) of the recordings shown in G. Each dots show the AUC of an individual cell.
Dots represent the result of an independent experiment; the histograms represent the mean and the bars the S.D. **, $p < 0.01$; ****, $p < 0.0001$ using Kruskal-Wallis test with Dunn's correction.

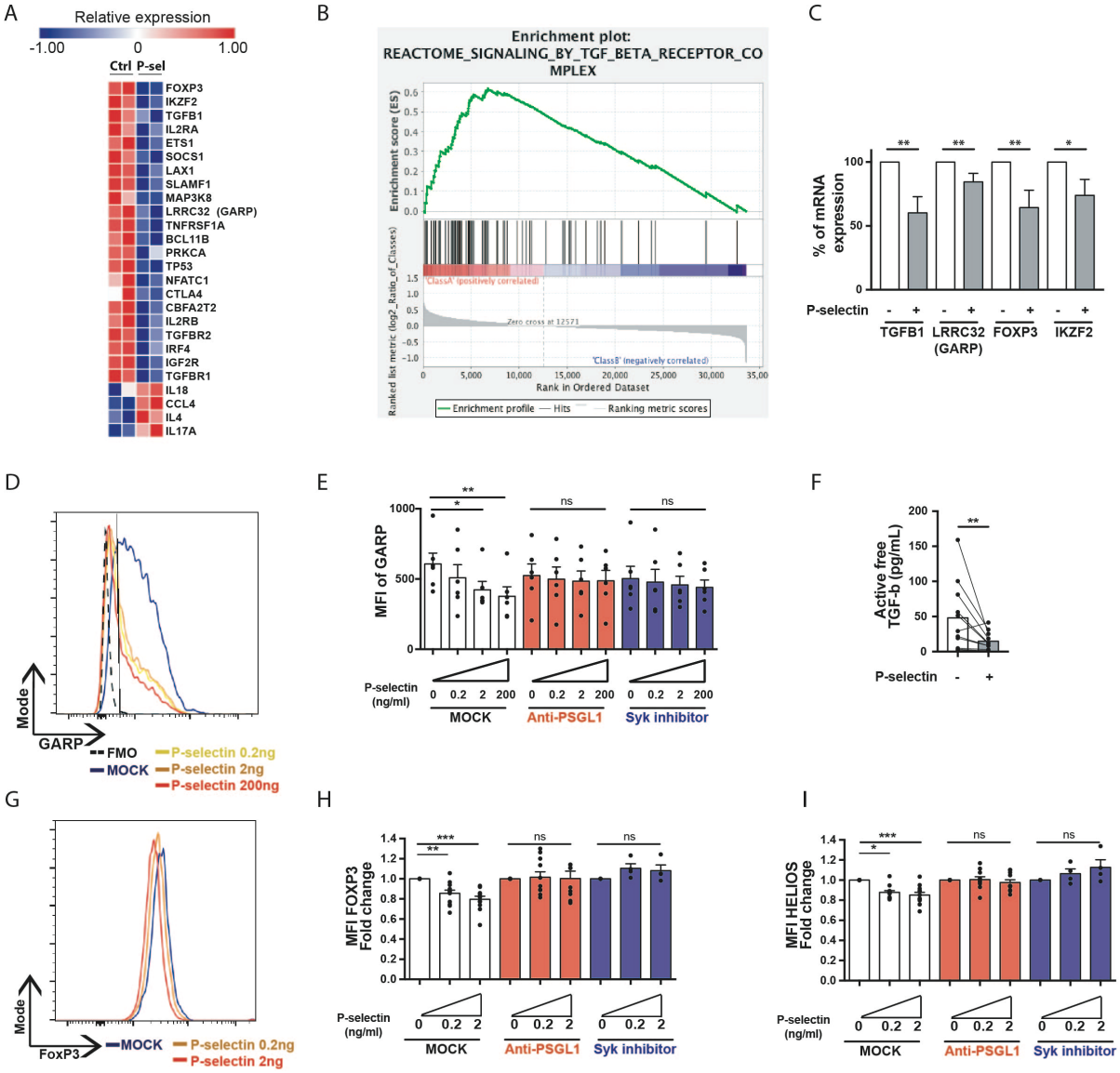

Figure 4: Selectins alter Treg phenotype through TGF-beta pathway modulation

(A) Heat map of selected gene showing a downregulation of Treg specific gene and upregulation of pro-inflammatory genes. Transcriptomics was conducted on a Affymetrix Nugen microarray using Tregs from 2 healthy donors treated for 8 hours with P-selectin 200pg/mL.

(B) GSEA analysis showing enrichment for TGF-beta signaling pathway in control Tregs compared with P-selectin treated Tregs.

(C) RT-qPCR of genes involved in the TGF-beta axis and FoxP3 signature. Tregs from 5 individual donors were cultured with or without P-selectin in the same conditions than transcriptomics. The results are given as a percentage of expression (ΔΔCT using a housekeeping gene) compared to the control. *, $p < 0.05$ and **, $p < 0.01$ using non parametric Mann-Whitney test.

(D) Tregs from HD were cultured during 48 hours with different dose of P-selectin with or without anti-PSGL1 (1/200) or Syk inhibitor (1 µM). Representative staining of GARP on viable Tregs.

(E) Cumulative data showing GARP MFI in Tregs cultured with P-selectin (n = 6 experiments).

(F) Free active TGF-beta was measured in the supernatant of Tregs culture with or without P-selectin (200pg/mL) for 48 hours (n = 11 independent experiments). **, $p < 0.01$ using the paired non-parametric Wilcoxon test.

(G) Tregs from HD were cultured during 48 hours with different dose of P-selectin with or without anti-PSGL1 (1/200) or Syk inhibitor (1 μM). Representative staining of FoxP3 on viable Tregs.

(H) Cumulative data showing FoxP3 MFI fold change in Tregs cultured with P-selectin under control condition (n = 12) of with anti-PSGL-1 antibody (1/200; n = 12) or Syk inhibitor (1μM, n = 4).

(I) Cumulative data showing Helios MFI fold change in Tregs cultured with P-selectin under control condition (n = 12) of with anti-PSGL-1 antibody (1/200; n = 12) or Syk inhibitor (1μM, n = 4).

Each dots represent the mean value of an independent experiment, histograms and bars represent the mean and the s.e.m. *, $p < 0.05$; **, $p < 0.01$; ***, $p < 0.001$ using non-parametric paired Friedman, test with Dunn's correction for multiple testing.

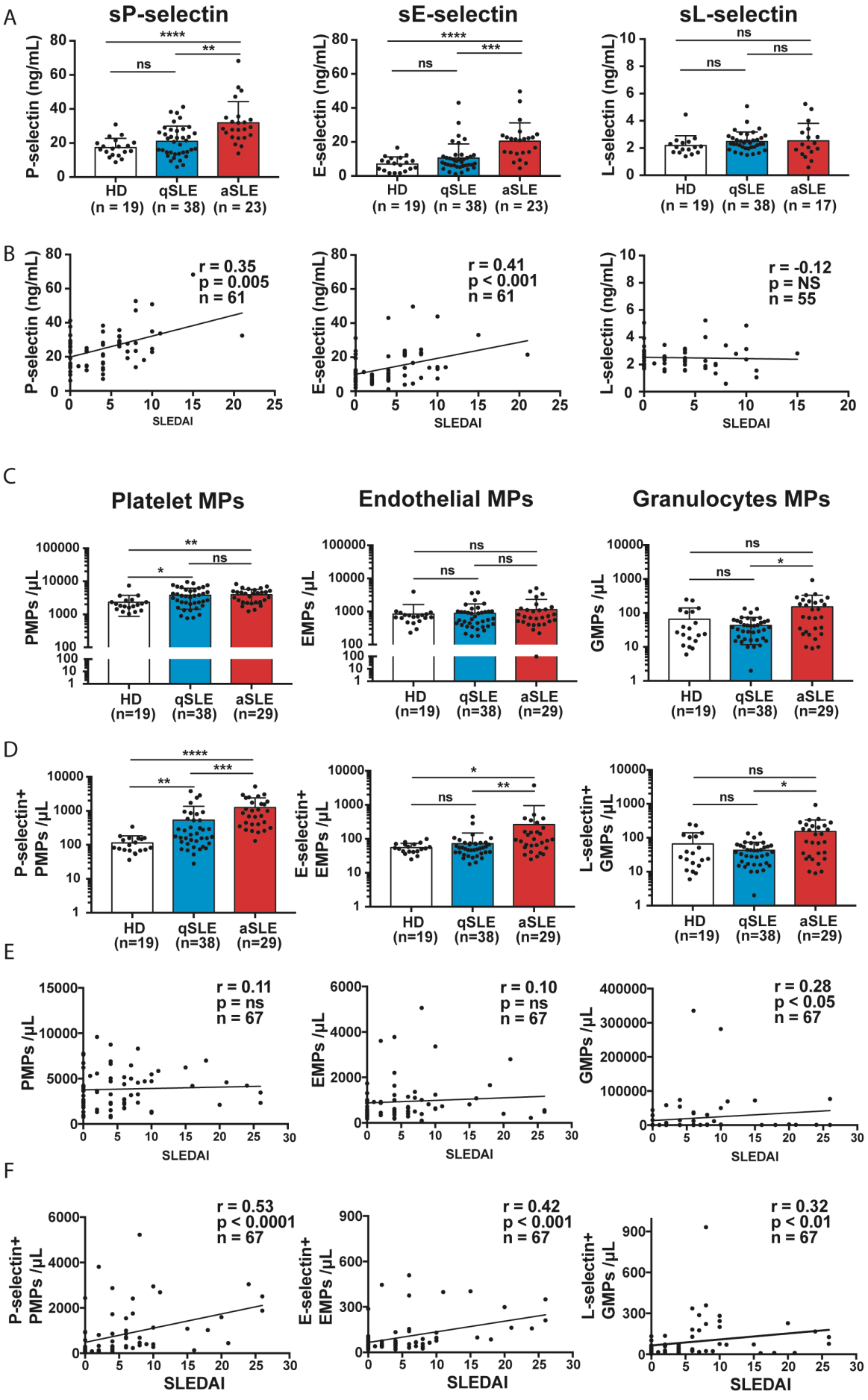
A
sP-selectin
sE-selectin
sL-selectin
P-selectin (ng/mL)
E-selectin (ng/mL)
L-selectin (ng/mL)
HD (n = 19)
qSLE (n = 38)
aSLE (n = 23)
aSLE (n = 17)
B
r = 0.35
p = 0.005
n = 61
r = 0.41
p < 0.001
n = 61
r = -0.12
p = NS
n = 55
SLEDAI
C
Platelet MPs
Endothelial MPs
Granulocytes MPs
PMPs /µL
EMPs /µL
GMPs /µL
HD (n=19)
qSLE (n=38)
aSLE (n=29)
D
P-selectin+ PMPs /µL
E-selectin+ EMPs /µL
L-selectin+ GMPs /µL
E
r = 0.11
p = ns
n = 67
r = 0.10
p = ns
n = 67
r = 0.28
p < 0.05
n = 67
F
r = 0.53
p < 0.0001
n = 67
r = 0.42
p < 0.001
n = 67
r = 0.32
p < 0.01
n = 67

1019

Figure 5: Soluble and microparticle-bound selectin are upregulated in active SLE patients

(A) Soluble selectins were measured from the platelet-free plasma of age- and sex-matched healthy donors, quiescent SLE (qSLE, SLEDAI < 6) and active SLE (aSLE, SLEDAI ≥6). Patients with active glomerulonephritis were excluded from this analysis (n = 6).

(B) Spearman correlation between selectin levels and SLE disease activity as assessed by the SLEDAI.

(C) Platelet-(CD61+, left panel), Endothelial- (CD31+, middle panel) or granulocyte-(CD66b+, right panel) derived Microparticles (PMP, EMP and GMP) were measured using cytometry from platelet-free plasma of HD and patients with quiescent or active SLE. The absolute count of microparticles was measured using Trucount Beads®.

(D) P-selectin+ PMPs, E-selectin+ EMPs and L-selectin+ GMPs were measured by cytometry from HD and SLE patients.

(E) Spearman correlation between PMPs (left panel), EMPs (middle panel) or GMPs (right panel) and SLE disease activity (SLEDAI).

(F) Spearman correlation between selectin^{+} PMPs (left panel), EMPs (middle panel) or GMPs (right panel) and SLE disease activity (SLEDAI).

Each dots represent the value of an individual, histograms and bars represent the mean and the S.D. $p < 0.05$; **, $p < 0.01$; ***, $p < 0.001$; ****, $p < 0.0001$ using non-parametric Kruskal-Wallis test with Dunn's correction for multiple testing.

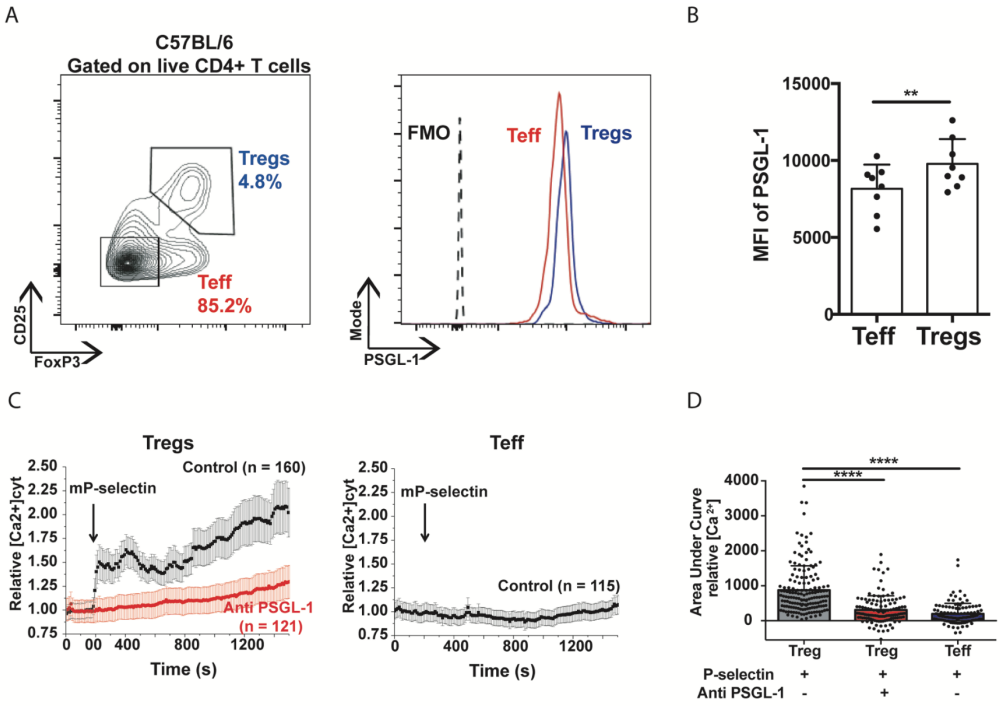
A
C57BL/6
Gated on live CD4+ T cells
Tregs
4.8%
Teff
85.2%
CD25
FoxP3
FMO
Teff
Tregs
Mode
PSGL-1
B
MFI of PSGL-1
15000
10000
5000
0
**
Teff
Tregs
C
Tregs
Control (n = 160)
mP-selectin
Anti PSGL-1
(n = 121)
Relative [Ca2+]cyt
Time (s)
Teff
mP-selectin
Control (n = 115)
Relative [Ca2+]cyt
Time (s)
D
Area Under Curve
relative [Ca2+]
****
****
Treg
Treg
Teff
P-selectin + + +
Anti PSGL-1 - + -

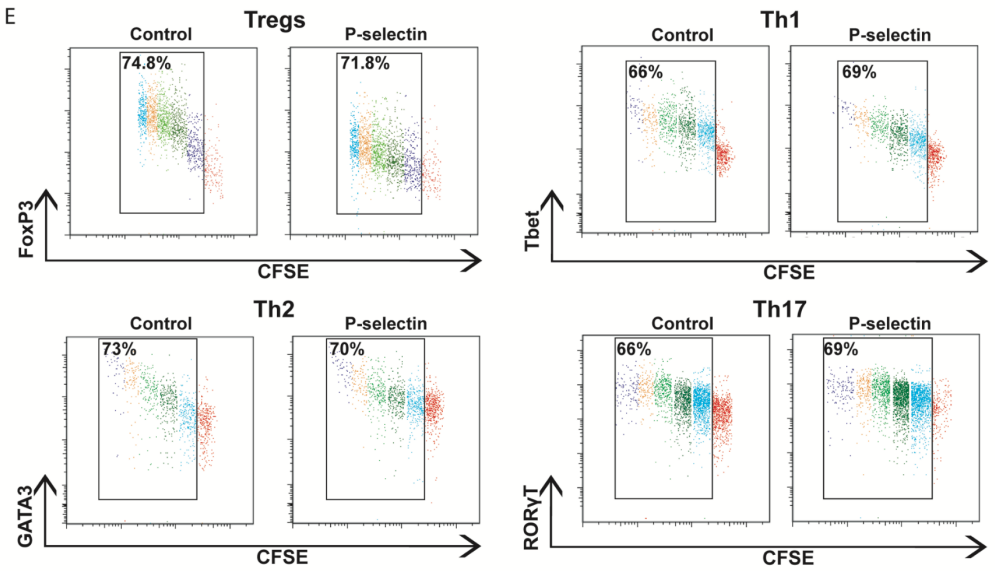
E
Tregs
Control
P-selectin
74.8%
71.8%
FoxP3
CFSE
Th1
Control
P-selectin
66%
69%
Tbet
CFSE
Th2
Control
P-selectin
73%
70%
GATA3
CFSE
Th17
Control
P-selectin
66%
69%
RORγT
CFSE

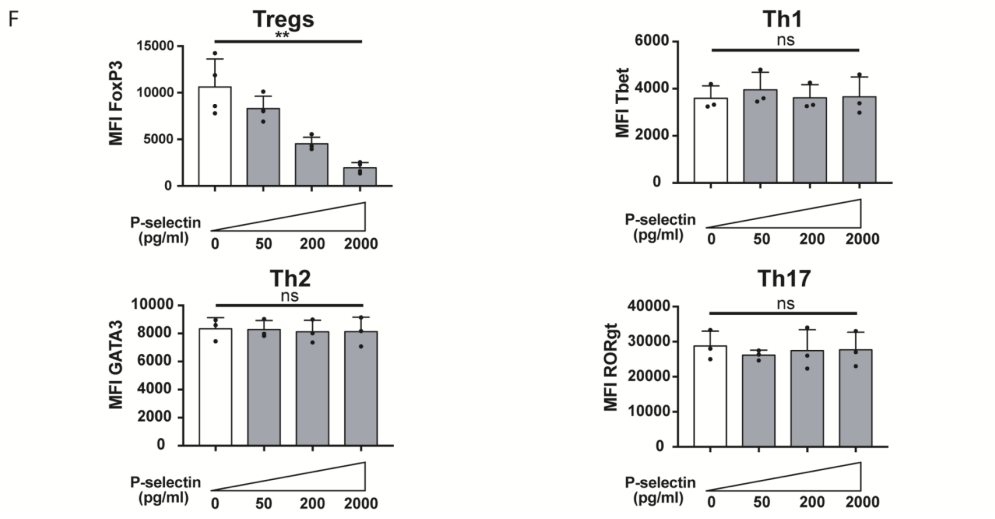
F
Tregs
**
MFI FoxP3
15000
10000
5000
0
P-selectin
(pg/ml)
0 50 200 2000
Th1
ns
MFI Tbet
6000
4000
2000
0
P-selectin
(pg/ml)
0 50 200 2000
Th2
ns
MFI GATA3
10000
8000
6000
4000
2000
0
P-selectin
(pg/ml)
0 50 200 2000
Th17
ns
MFI RORgt
40000
30000
20000
10000
0
P-selectin
(pg/ml)
0 50 200 2000

1070

Figure 6: WT and dnase1l3-KO with CD57B/6 background recapitulate human P-selectin findings

(A) Gating strategy of FoxP3$^+$ Tregs and Teff extracted from the spleen of C57/B6 WT mice (n = 8).

(B) Cumulative results of PSGL-1 expression on Teff and Tregs (n = 8). **, $p < 0.01$ using matched non-parametric Wilcoxon test.

(C) CD25+CD4+ Tregs (left panel) or CD25-CD4+ Teff (right panel) were incubated with recombinant mouse P-selectin with or without pre-treatment with mouse anti-PSGL1 antibody. Single-cell normalized intracytosolic calcium concentration ($[Ca^{2+}]_{cyt}$ using cal-520 as fluorescent calcium probe). The n shows the number of cells evaluated in each conditions. The data were obtained from three independent experiments.

(D) Area under curve of calcium levels in cells exposed to P-selectin. Each dots represent the AUC of a single cells.

(E) Naïve CD62L$^+$ CD4$^+$ mouse T cells were stained with CFSE and cultured under polarizing conditions for Treg, Th1, Th2 and Th17 differentiation, with or without P-selectin. Representative staining of CFSE and differentiation transcription factor after 7 days of incubation. The percentage indicates the proportion of proliferating cells.

(F) Mean fluorescence intensity of the transcription factor of differentiation for each polarizing conditions.

Each dot represent the value of one mouse or one independent experiment with means and S.D.**, $p < 0.01$; ****, $p < 0.0001$ using non-parametric Kruskal-Wallis test with Dunn's correction for multiple testing.

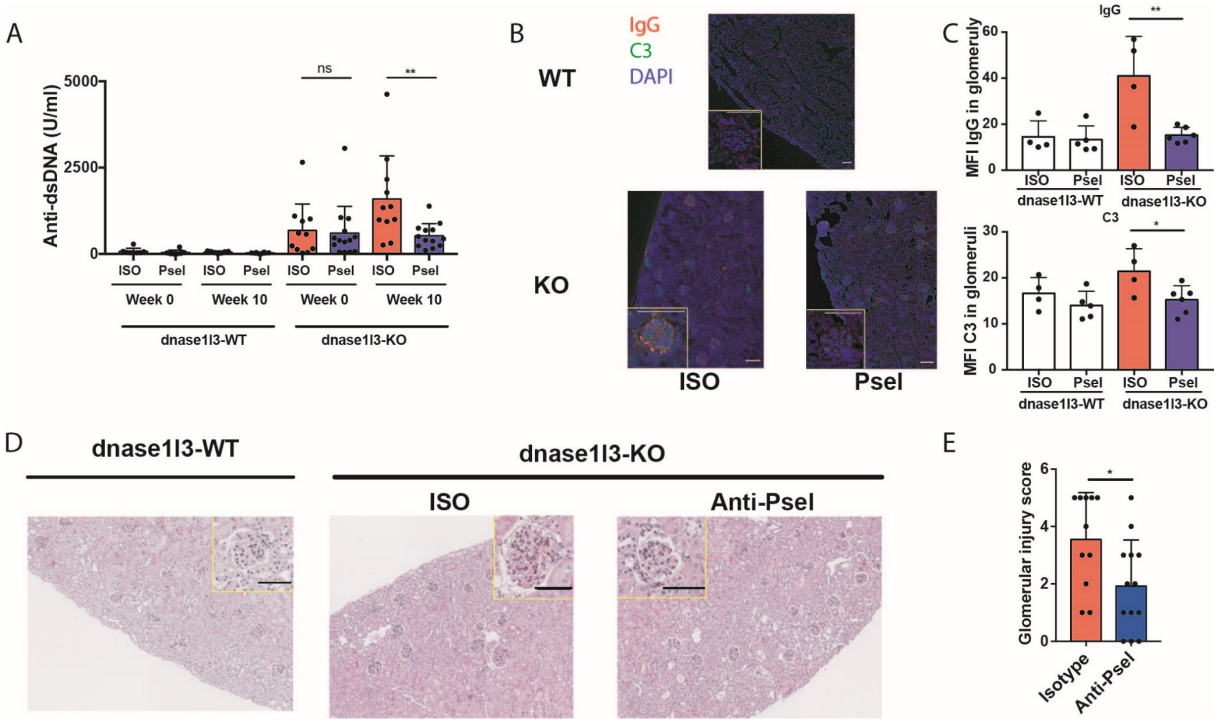

Figure 7: P-selectin blockade improves SLE pathogenesis in *dnase1l3-KO* lupus-prone mice.

(A) Levels of anti-dsDNA antibodies in dnase1l3-KO mice measured by ELISA of two independent experiments (WT mice, n = 7 in ISO group and n = 8 in anti-Psel group; for KO mice, n = 11 in the ISO group and n = 13 in anti-Psel group).

(B) Representative Immunofluorescence staining of kidney of dnase1l3-WT (upper panel) and dnase1l3-KO mouse treated with the isotype (lower left panel) or the anti-P-selectin (lower right panel) antibody for 10 weeks. White bars indicate 100 µm.

(C) Cumulative results of the MFI of IgG (upper panel) and C3 (lower panel) in the glomeruli of dnase1l3-WT and dnase1l3-KO mice treated with the isotype or the anti-P-selectin antibody.

(D) Representative HES staining of kidney of dnase1l3-WT and dnase1l3-KO mice treated with the isotype of the anti-P-selectin antibody for 10 weeks. Black bars indicate 50 µm.

(E) Glomerular injury score evaluated in a blinded manner by a kidney pathologist, as described in the *methods*.

Each dot represents the value of one mouse with means and S.D. *, $p < 0.05$; **, $p < 0.01$ using unpaired Student's t-test.

References :

1. G. C. Tsokos, Systemic lupus erythematosus, *N. Engl. J. Med.* **365**, 2110–2121 (2011).

2. E. Lazaro, M. Scherlinger, M.-E. Truchetet, L. Chiche, T. Schaeverbeke, P. Blanco, C. Richez, Biotherapies in systemic lupus erythematosus: New targets, *Joint Bone Spine* **84**, 267–274 (2017).

3. K. Ohl, K. Tenbrock, Regulatory T cells in systemic lupus erythematosus, *Eur. J. Immunol.* **45**, 344–355 (2015).

4. C. Jacquemin, N. Schmitt, C. Contin-Bordes, Y. Liu, P. Narayanan, J. Seneschal, T. Maurouard, D. Dougall, E. S. Davizon, H. Dumortier, I. Douchet, L. Raffray, C. Richez, E. Lazaro, P. Duffau, M.-E. Truchetet, L. Khoryati, P. Mercié, L. Couzi, P. Merville, T. Schaeverbeke, J.-F. Viallard, J.-L. Pellegrin, J.-F. Moreau, S. Muller, S. Zurawski, R. L. Coffman, V. Pascual, H. Ueno, P. Blanco, OX40 Ligand Contributes to Human Lupus Pathogenesis by Promoting T Follicular Helper Response, *Immunity* **42**, 1159–1170 (2015).

5. L. Pattarini, C. Trichot, S. Bogiatzi, M. Grandclaudon, S. Meller, Z. Keuylian, M. Durand, E. Volpe, S. Madonna, A. Cavani, A. Chiricozzi, M. Romanelli, T. Hori, A. Hovnanian, B. Homey, V. Soumelis, TSLP-activated dendritic cells induce human T follicular helper cell differentiation through OX40-ligand, *J. Exp. Med.* **214**, 1529–1546 (2017).

6. C. Jacquemin, J.-F. Augusto, M. Scherlinger, N. Gensous, E. Forcade, I. Douchet, E. Levionnois, C. Richez, E. Lazaro, P. Duffau, M.-E. Truchetet, J. Seneschal, L. Couzi, J.-L. Pellegrin, J.-F. Viallard, T. Schaeverbeke, V. Pascual, C. Contin-Bordes, P. Blanco, OX40L/OX40 axis impairs follicular and natural Treg function in human SLE, *JCI Insight* **3** (2018), doi:10.1172/jci.insight.122167.

7. O. Olumuyiwa-Akeredolu, M. J. Page, P. Soma, E. Pretorius, Platelets: emerging facilitators of cellular crosstalk in rheumatoid arthritis, *Nat. Rev. Rheumatol.* **15**, 237–248 (2019).

8. M. Scherlinger, V. Guillotin, M.-E. Truchetet, C. Contin-Bordes, V. Sisirak, P. Duffau, E. Lazaro, C. Richez, P. Blanco, Systemic lupus erythematosus and systemic sclerosis: All roads lead to platelets, *Autoimmun. Rev.* **17**, 625–635 (2018).

9. P. Duffau, J. Seneschal, C. Nicco, C. Richez, E. Lazaro, I. Douchet, C. Bordes, J.-F. Viallard, C. Goulvestre, J.-L. Pellegrin, B. Weil, J.-F. Moreau, F. Batteux, P. Blanco, Platelet CD154 Potentiates Interferon- Secretion by Plasmacytoid Dendritic Cells in Systemic Lupus Erythematosus, *Sci. Transl. Med.* **2**, 47ra63-47ra63 (2010).

10. G. I. Johnston, G. A. Bliss, P. J. Newman, R. P. McEver, Structure of the human gene encoding granule membrane protein-140, a member of the selectin family of adhesion receptors for leukocytes., *J. Biol. Chem.* **265**, 21381–21385 (1990).

11. S. J. Bielinski, C. Berardi, P. A. Decker, P. S. Kirsch, N. B. Larson, J. S. Pankow, M. Sale, M. de Andrade, H. Sicotte, W. Tang, N. Q. Hanson, C. L. Wassel, J. F. Polak, M. Y. Tsai, P-selectin and subclinical and clinical atherosclerosis: the Multi-Ethnic Study of Atherosclerosis (MESA), *Atherosclerosis* **240**, 3–9 (2015).

12. N. I. Shapiro, P. Schuetz, K. Yano, M. Sorasaki, S. M. Parikh, A. E. Jones, S. Trzeciak, L. Ngo, W. C. Aird, The association of endothelial cell signaling, severity of illness, and organ dysfunction in sepsis, *Crit. Care* **14**, R182 (2010).

13. M. Tsokos, F. Fehlauer, K. Püschel, Immunohistochemical expression of E-selectin in sepsis-induced lung injury, *Int. J. Legal Med.* **113**, 338–342 (2000).

14. M. Silva, R. K. F. Fung, C. B. Donnelly, P. A. Videira, R. Sackstein, Cell-Specific Variation in E-Selectin Ligand Expression among Human Peripheral Blood Mononuclear Cells: Implications for Immunosurveillance and Pathobiology, *J. Immunol.* **198**, 3576–3587 (2017).

15. R. J. Johnston, L. J. Su, J. Pinckney, D. Critton, E. Boyer, A. Krishnakumar, M. Corbett, A. L. Rankin, R. Dibella, L. Campbell, G. H. Martin, H. Lemar, T. Cayton, R. Y.-C. Huang, X. Deng, A. Nayeem, H. Chen, B. Ergel, J. M. Rizzo, A. P. Yamniuk, S. Dutta, J. Ngo, A. O. Shorts, R. Ramakrishnan, A. Kozhich, J. Holloway, H. Fang, Y.-K. Wang, Z. Yang, K. Thiam, G. Rakestraw, A. Rajpal, P. Sheppard, M. Quigley, K. S. Bahjat, A. J. Korman, VISTA is an acidic pH-selective ligand for PSGL-1, *Nature* **574**, 565–570 (2019).

16. R. Tinoco, F. Carrette, M. L. Barraza, D. C. Otero, J. Magaña, M. W. Bosenberg, S. L. Swain, L. M. Bradley, PSGL-1 is an immune checkpoint regulator that promotes T cell exhaustion, *Immunity* **44**, 1190–1203 (2016).

17. M. Miyara, D. Chader, E. Sage, D. Sugiyama, H. Nishikawa, D. Bouvry, L. Claër, R. Hingorani, R. Balderas, J. Rohrer, N. Warner, A. Chapelier, D. Valeyre, R. Kannagi, S. Sakaguchi, Z. Amoura, G. Gorochov, Sialyl Lewis x (CD15s) identifies highly differentiated and most suppressive FOXP3 ^{high} regulatory T cells in humans, *Proc. Natl. Acad. Sci.* **112**, 7225–7230 (2015).

18. K. I. Hidari, A. S. Weyrich, G. A. Zimmerman, R. P. McEver, Engagement of P-selectin glycoprotein ligand-1 enhances tyrosine phosphorylation and activates mitogen-activated protein kinases in human neutrophils, *J. Biol. Chem.* **272**, 28750–28756 (1997).

19. A. Urzainqui, J. M. Serrador, F. Viedma, M. Yáñez-Mó, A. Rodríguez, A. L. Corbí, J. L. Alonso-Lebrero, A. Luque, M. Deckert, J. Vázquez, F. Sánchez-Madrid, ITAM-Based Interaction of ERM Proteins with Syk Mediates Signaling by the Leukocyte Adhesion Receptor PSGL-1, *Immunity* **17**, 401–412 (2002).

20. A. Mócsai, J. Ruland, V. L. J. Tybulewicz, The SYK tyrosine kinase: a crucial player in diverse biological functions, *Nat. Rev. Immunol.* **10**, 387–402 (2010).

21. L. Sun, H. Jin, H. Li, GARP: a surface molecule of regulatory T cells that is involved in the regulatory function and TGF-β releasing, *Oncotarget* **7**, 42826–42836 (2016).

22. T. Wu, C. Xie, H. W. Wang, X. J. Zhou, N. Schwartz, S. Calixto, M. Mackay, C. Aranow, C. Putterman, C. Mohan, Elevated urinary VCAM-1, P-selectin, soluble TNF receptor-1, and CXC chemokine ligand 16 in multiple murine lupus strains and human lupus nephritis, *J. Immunol. Baltim. Md 1950* **179**, 7166–7175 (2007).

23. V. Sisirak, B. Sally, V. D'Agati, W. Martinez-Ortiz, Z. B. Özçakar, J. David, A. Rashidfarrokhi, A. Yeste, C. Panea, A. S. Chida, M. Bogunovic, I. I. Ivanov, F. J. Quintana, I. Sanz, K. B. Elkon, M. Tekin, F. Yalçınkaya, T. J. Cardozo, R. M. Clancy, J. P. Buyon, B.

Reizis, Digestion of Chromatin in Apoptotic Cell Microparticles Prevents Autoimmunity, *Cell* **166**, 88–101 (2016).

24. A. Oyler-Yaniv, J. Oyler-Yaniv, B. M. Whitlock, Z. Liu, R. N. Germain, M. Huse, G. Altan-Bonnet, O. Krichevsky, A Tunable Diffusion-Consumption Mechanism of Cytokine Propagation Enables Plasticity in Cell-to-Cell Communication in the Immune System, *Immunity* **46**, 609–620 (2017).

25. J. T. Cortez, E. Montauti, E. Shifrut, J. Gatchalian, Y. Zhang, O. Shaked, Y. Xu, T. L. Roth, D. R. Simeonov, Y. Zhang, S. Chen, Z. Li, J. M. Woo, J. Ho, I. A. Vogel, G. Y. Prator, B. Zhang, Y. Lee, Z. Sun, I. Ifergan, F. Van Gool, D. C. Hargreaves, J. A. Bluestone, A. Marson, D. Fang, CRISPR screen in regulatory T cells reveals modulators of Foxp3, *Nature* **582**, 416–420 (2020).

26. D. Haribhai, X. Luo, J. Chen, S. Jia, L. Shi, J. A. Schroeder, H. Weiler, R. H. Aster, M. J. Hessner, J. Hu, C. B. Williams, Q. Shi, TGF-β1 along with other platelet contents augments Treg cells to suppress anti-FVIII immune responses in hemophilia A mice, *Blood Adv.* **1**, 139–151 (2016).

27. W. Li, C. Deng, H. Yang, G. Wang, The Regulatory T Cell in Active Systemic Lupus Erythematosus Patients: A Systemic Review and Meta-Analysis, *Front. Immunol.* **10** (2019), doi:10.3389/fimmu.2019.00159.

28. X. Pan, X. Yuan, Y. Zheng, W. Wang, J. Shan, F. Lin, G. Jiang, Y. H. Yang, D. Wang, D. Xu, L. Shen, Increased CD45RA+FoxP3low Regulatory T Cells with Impaired Suppressive Function in Patients with Systemic Lupus Erythematosus, *PLoS ONE* **7** (2012), doi:10.1371/journal.pone.0034662.

29. J. Y. Humrich, C. von Spee-Mayer, E. Siegert, M. Bertolo, A. Rose, D. Abdirama, P. Enghard, B. Stuhlmüller, B. Sawitzki, D. Huscher, F. Hiepe, T. Alexander, E. Feist, A. Radbruch, G.-R. Burmester, G. Riemekasten, Low-dose interleukin-2 therapy in refractory systemic lupus erythematosus: an investigator-initiated, single-centre phase 1 and 2a clinical trial, *Lancet Rheumatol.* **1**, e44–e54 (2019).

30. M. Rosenzwajg, R. Lorenzon, P. Cacoub, H. P. Pham, F. Pitoiset, K. El Soufi, C. RIbet, C. Bernard, S. Aractingi, B. Banneville, L. Beaugerie, F. Berenbaum, J. Champey, O. Chazouilleres, C. Corpechot, B. Fautrel, A. Mekinian, E. Regnier, D. Saadoun, J.-E. Salem, J. Sellam, P. Seksik, A. Daguenel-Nguyen, V. Doppler, J. Mariau, E. Vicaut, D. Klatzmann, Immunological and clinical effects of low-dose interleukin-2 across 11 autoimmune diseases in a single, open clinical trial, *Ann. Rheum. Dis.* **78**, 209–217 (2019).

31. K. Nakatani, H. Fujii, H. Hasegawa, M. Terada, N. Arita, M. R. Ito, M. Ono, S. Takahashi, K. Saiga, S. Yoshimoto, M. Iwano, H. Shiiki, Y. Saito, M. Nose, Endothelial adhesion molecules in glomerular lesions: Association with their severity and diversity in lupus models, *Kidney Int.* **65**, 1290–1300 (2004).

32. A. Urzainqui, G. Martínez del Hoyo, A. Lamana, H. de la Fuente, O. Barreiro, I. M. Olazabal, P. Martin, M. K. Wild, D. Vestweber, R. González-Amaro, F. Sánchez-Madrid, Functional role of P-selectin glycoprotein ligand 1/P-selectin interaction in the generation of tolerogenic dendritic cells, *J. Immunol. Baltim. Md 1950* **179**, 7457–7465 (2007).

33. J. Etulain, K. Martinod, S. L. Wong, S. M. Cifuni, M. Schattner, D. D. Wagner, P-selectin promotes neutrophil extracellular trap formation in mice, *Blood* **126**, 242–246 (2015).

34. J. Suzuki, E. Hamada, T. Shodai, G. Kamoshida, S. Kudo, S. Itoh, J. Koike, K. Nagata, T. Irimura, T. Tsuji, Cytokine Secretion from Human Monocytes Potentiated by P-Selectin-Mediated Cell Adhesion, *Int. Arch. Allergy Immunol.* **160**, 152–160 (2013).

35. J. W. Semple, J. E. Italiano, J. Freedman, Platelets and the immune continuum, *Nat. Rev. Immunol.* **11**, 264–274 (2011).

36. R. Kapur, A. Zufferey, E. Boilard, J. W. Semple, Nouvelle Cuisine: Platelets Served with Inflammation, *J. Immunol.* **194**, 5579–5587 (2015).

37. P. Linge, P. R. Fortin, C. Lood, A. A. Bengtsson, E. Boilard, The non-haemostatic role of platelets in systemic lupus erythematosus, *Nat. Rev. Rheumatol.* **14**, 195–213 (2018).

38. E. Boilard, P. A. Nigrovic, K. Larabee, G. F. M. Watts, J. S. Coblyn, M. E. Weinblatt, E. M. Massarotti, E. Remold-O'Donnell, R. W. Farndale, J. Ware, D. M. Lee, Platelets amplify inflammation in arthritis via collagen-dependent microparticle production, *Science* **327**, 580–583 (2010).

39. P. Han, D. Hanlon, N. Arshad, J. S. Lee, K. Tatsuno, E. Robinson, R. Filler, O. Sobolev, C. Cote, F. Rivera-Molina, D. Toomre, T. Fahmy, R. Edelson, Platelet P-selectin initiates cross-presentation and dendritic cell differentiation in blood monocytes, *Sci. Adv.* **6**, eaaz1580 (2020).

40. N. Nanda, P. Andre, M. Bao, K. Clauser, F. Deguzman, D. Howie, P. B. Conley, C. Terhorst, D. R. Phillips, Platelet aggregation induces platelet aggregate stability via SLAM family receptor signaling, *Blood* **106**, 3028–3034 (2005).

41. Y. Wang, H. Gao, C. Shi, P. W. Erhardt, A. Pavlovsky, D. A Soloviev, K. Bledzka, V. Ustinov, L. Zhu, J. Qin, A. D. Munday, J. Lopez, E. Plow, D. I. Simon, Leukocyte integrin Mac-1 regulates thrombosis via interaction with platelet GPIbα, *Nat. Commun.* **8**, 15559 (2017).

42. M. Mezger, H. Nording, R. Sauter, T. Graf, C. Heim, N. von Bubnoff, S. M. Ensminger, H. F. Langer, Platelets and Immune Responses During Thromboinflammation, *Front. Immunol.* **10** (2019), doi:10.3389/fimmu.2019.01731.

43. S. Rachidi, A. Metelli, B. Riesenberg, B. X. Wu, M. H. Nelson, C. Wallace, C. M. Paulos, M. P. Rubinstein, E. Garrett-Mayer, M. Hennig, D. W. Bearden, Y. Yang, B. Liu, Z. Li, Platelets subvert T cell immunity against cancer via GARP-TGFβ axis, *Sci. Immunol.* **2** (2017), doi:10.1126/sciimmunol.aai7911.

44. M. Giannelou, C. P. Mavragani, Cardiovascular disease in systemic lupus erythematosus: A comprehensive update, *J. Autoimmun.* **82**, 1–12 (2017).

45. B. J. Skaggs, B. H. Hahn, M. McMahon, Accelerated atherosclerosis in patients with SLE—mechanisms and management, *Nat. Rev. Rheumatol.* **8**, 214–223 (2012).

46. D. E. Gaddis, L. E. Padgett, R. Wu, C. McSkimming, V. Romines, A. M. Taylor, C. A. McNamara, M. Kronenberg, S. Crotty, M. J. Thomas, M. G. Sorci-Thomas, C. C. Hedrick,

Apolipoprotein AI prevents regulatory to follicular helper T cell switching during atherosclerosis, *Nat. Commun.* **9** (2018), doi:10.1038/s41467-018-03493-5.

47. P. C. Burger, D. D. Wagner, Platelet P-selectin facilitates atherosclerotic lesion development, *Blood* **101**, 2661–2666 (2003).

48. K. I. Ataga, A. Kutlar, J. Kanter, D. Liles, R. Cancado, J. Friedrisch, T. H. Guthrie, J. Knight-Madden, O. A. Alvarez, V. R. Gordeuk, S. Gualandro, M. P. Colella, W. R. Smith, S. A. Rollins, J. W. Stocker, R. P. Rother, Crizanlizumab for the Prevention of Pain Crises in Sickle Cell Disease, *N. Engl. J. Med.* **376**, 429–439 (2017).

49. N. Arraud, R. Linares, S. Tan, C. Gounou, J.-M. Pasquet, S. Mornet, A. R. Brisson, Extracellular vesicles from blood plasma: determination of their morphology, size, phenotype and concentration, *J. Thromb. Haemost.* **12**, 614–627 (2014).